**NOAA NESDIS
CENTER for SATELLITE APPLICATIONS and
RESEARCH**

ALGORITHM THEORETICAL BASIS DOCUMENT

Enterprise AWG Cloud Height Algorithm (ACHA)

Andrew Heidinger, NOAA/NESDIS/STAR
Yue Li, CIMSS/SSEC
Steve Wanzong, CIMSS/SSEC

Version 3.4
September, 2020

TABLE OF CONTENTS

3

4

LIST OF FIGURES

6

particle size from the final retrieved β values.

7

LIST OF TABLES

LIST OF ACRONYMS

1DVAR - one-dimensional variational
ABI - Advanced Baseline Imager
AHI - Advanced Himawari Imager
AIADD - Algorithm Interface and Ancillary Data Description
AIT - Algorithm Integration Team
ATBD - Algorithm Theoretical Basis Document
A-Train - Afternoon Train (Aqua, CALIPSO, CloudSat, etc.)
AVHRR - Advanced Very High Resolution Radiometer
AWG - Algorithm Working Group
BT - Brightness Temperature
BTD - Brightness Temperature Difference
CALIPSO - Cloud-Aerosol Lidar and Infrared Pathfinder Satellite
CIMSS - Cooperative Institute for Meteorological Satellite Studies
CLAVR-x - Clouds from the Advanced Very High Resolution Radiometer (AVHRR) Extended
CRTM - Community Radiative Transfer Model (CRTM), currently under development.
ECMWF - European Centre for Medium-Range Weather Forecasts
EOS - Earth Observing System
EUMETSAT- European Organization for the Exploitation of Meteorological Satellites
F&PS - Function and Performance Specification
GFS - Global Forecast System
GOES - Geostationary Operational Environmental Satellite
GOES-RRR – GOES-R Risk Reduction
IR - Infrared
IRW - IR Window
ISCCP - International Satellite Cloud Climatology Project
JPSS - Joint Polar Satellite System
MODIS - Moderate Resolution Imaging Spectroradiometer
MSG - Meteosat Second Generation
NASA - National Aeronautics and Space Administration
NESDIS - National Environmental Satellite, Data, and Information Service
NOAA - National Oceanic and Atmospheric Administration
NWP - Numerical Weather Prediction
PFAAST - Pressure layer Fast Algorithm for Atmospheric Transmittances
PLOD - Pressure Layer Optical Dept
POES - Polar Orbiting Environmental Satellite
RTM - Radiative Transfer Model
SEVIRI - Spinning Enhanced Visible and Infrared Imager
S-NPP - Suomi National Polar-orbiting Partnership
SSEC - Space Science and Engineering Center
STAR - Center for Satellite Applications and Research

11
VIIRS - Visible Infrared Imager Radiometer Suite
UW - University of Wisconsin at Madison

1 ABSTRACT

This document describes the algorithm for the GOES-R ABI Cloud Height Algorithm (ACHA). ACHA has been made flexible to run various sensors including MODIS, VIIRS, GOES-16/17 ABI, etc. The ACHA generates the cloud-top height, cloud-top temperature, cloud-top pressure and cloud layer products. The ACHA uses only infrared observations in order to provide products that are consistent for day, night and terminator conditions. The ACHA uses an analytical model of infrared radiative transfer embedded into an optimal estimation retrieval methodology. Cloud-top pressure and cloud-top height are derived from the cloud-top temperature product and the atmospheric temperature profile provided by Numerical Weather Prediction (NWP) data. The cloud layer product is derived solely from the cloud-top pressure product.

The ACHA uses the spectral information provided by the GOES-R ABI to derive cloud-top height information simultaneously with cloud microphysical information. In discussion of retrievals from the GOES-R ABI in this document, the ACHA employs the 11, 12 and 13.3 μm observations. This information allows the ACHA to avoid making assumptions on cloud microphysics in the retrieval of cloud height. As a consequence, ACHA also generates the intermediate products of 11.2 μm cloud emissivity and an 11/12 μm microphysical index. Additionally, ice cloud fraction, the lower level cloud top information under cloud-overlapping conditions, and infrared based cloud optical properties, such as cloud optical depth and particle size, are also retrieved.

This document will describe the required inputs, the theoretical foundation of the algorithms, the sources and magnitudes of the errors involved, practical considerations for implementation, and the assumptions and limitations associated with the product, as well as provide a high level description of the physical basis for estimating the height of tops of clouds observed by the ABI. The results from running the ACHA on MODIS, which served as a proxy for VIIRS, validated against the CALIOP LIDAR as well as a comparison to the MODIS MYD06 Cloud height product are also shown.

2 INTRODUCTION

2.1 Purpose of This Document

The primary purpose of this ATBD is to establish guidelines for producing the cloud-top height, cloud-top temperature and cloud-top pressure from the ABI flown on the GOES-R series of NOAA geostationary meteorological satellites. This ATBD is written with an ABI slant, but most of it applies to the other sensors that ACHA supports (see Table 3 below). Only the L1b input combinations would change. This document will describe the required inputs, the theoretical foundation of the algorithms, the sources and magnitudes of the errors involved, practical considerations for implementation, and the assumptions and limitations associated with the product, as well as provide a high level description of the physical basis for estimating the height of the tops of clouds observed by the ABI. Unless otherwise stated, the determination of cloud-top height always implies the simultaneous determination of temperature and pressure. The cloud-top height is made available to all subsequent algorithms which require knowledge of the vertical extent of the clouds. The cloud-top height also plays a critical role in determining the cloud cover and layers product.

2.2 Who Should Use This Document

The intended users of this document are those interested in understanding the physical basis of the algorithms and how to use the output of this algorithm to optimize the cloud height output for a particular application. This document also provides information useful to anyone maintaining or modifying the original algorithm.

2.3 Inside Each Section

This document is broken down into the following main sections:

- **System Overview**: provides relevant details of the ABI and provides a brief description of the products generated by the algorithm.
- **Algorithm Description**: provides a detailed description of the algorithm including its physical basis, its input and its output.
- **Assumptions and Limitations**: provides an overview of the current limitations of the approach and notes plans for overcoming these limitations with further algorithm development.

2.4 Related Documents

This document currently does not relate to any other document outside of the specifications of the GOES-R F&PS and to the references given throughout.

2.5 Revision History

Initial Version 2.0 of this document was created by Dr. Andrew Heidinger of NOAA/NESDIS and its intent was to accompany the delivery of the version 4 algorithm to the GOES-R AWG AIT. This document was then revised following the document guidelines provided by the GOES-R Algorithm Application Group (AWG) before the version 0.5 delivery. Version 1.0 of the document includes some new results from the algorithm Critical Design Review (CDR) and the Test Readiness Review (TRR), as well as the algorithm 80% readiness document.

Version 3.0 is prepared by Dr. Yue Li to reflect the following changes: 1) combination of sounder and imager data for a better estimation of first guess values and uncertainties; 2) revision to ACHA mode numbers to make it consistent with current science codes; 3) introduction to the fusion method and a new ACHA mode; 4) adding description of off-diagonal components for forward model error covariance matrix; 5) adding discussion of infrared retrieved cloud optical properties; 6) rewriting the validation parts for VIIRS; 7) description on deriving a new radiometric-consistent ice microphysical model; 8) updates on lapse rate computation over water surfaces. Some outdated and/or inconsistent information in this document is also updated.

Version 3.1 revises a large part of the equations to reflect the changes to ACHA by introducing the lower level cloud top temperature under multilayer cloud condition as an additional output from ACHA's optimal estimation approach, instead of interpolating from surrounding water phase clouds. There are also updates for a better ice cloud first guess temperature, and extending the lapse rate method to estimate cloud top height over land surfaces.

Version 3.2 has some minor changes to reflect recent improvement to ACHA, including more supported channel combinations (modes) and updates to the ice crystal habits.

Version 3.3 has some major changes: 1) support of combinations of multiple channels including the following: $3.75\,\mu m$, $6.2\,\mu m$, $6.7\,\mu m$, $7.3\,\mu m$, $8.5\,\mu m$, $10.4\,\mu m$, $11\,\mu m$, $12\,\mu m$, $13.3\,\mu m$, $13.6\,\mu m$, $13.9\,\mu m$, $14.2\,\mu m$; 2) flexibility of using $10.4\,\mu m$ to replace $11\,\mu m$ observations (GOES-17 only); 3) changes of microphysical index β fitting from linear to high order polynomial to account for multiple scattering impact of the $3.75\,\mu m$; 4) including ice fraction as the fifth output from the optimal estimation algorithm.

In Version 3.4, changes are made to reflect all current supported channel combinations and include in Appendix A the GOES17 mitigation work. Some other updates such as use of the KD-tree technique and NUCAPS data are also briefly discussed.

3 OBSERVING SYSTEM OVERVIEW

This section describes the products generated by the ABI Cloud Height Algorithm (ACHA) and its associated sensor requirements.

3.1 Products Generated

The ACHA is responsible for estimation of vertical extent for all cloudy ABI pixels. In terms of the F&PS, it is responsible directly for the Cloud-Top Pressure, Height and Temperature products. The cloud height is also used to generate a cloud-layer flag which classifies a cloud as being a high, middle or low-level cloud. This flag is used in generating the cloud-cover layers product. The ACHA results are currently used in the daytime and nighttime cloud optical and microphysical algorithms. In addition, cloud-top pressure results from this algorithm are used in the Atmospheric Motion Vector (AMV) algorithm.

In addition to the cloud height metrics (pressure/temperature/height), the ACHA also provides an estimate of the 11 μm cloud emissivity and a microphysical parameter, β , derived from multiple emissivities that are related to particle size. These products, as described later, are generated automatically by the ACHA and are useful for evaluating the ACHA's performance. Additionally, two other retrieval parameters, the lower level cloud top temperature under multilayer cloud conditions and ice cloud fraction are provided. The requirements for the ACHA from the F&PS version 2.2 are stated below in Table 1, with height, pressure, temperature, layer from top to bottom for each geographic coverage.

Table 1 *Requirements from GOES-R F&PS version 2.2 for Cloud Top Parameters (Temperature, Pressure and Height). Specifications apply to clouds with 11 μm emissivities > 0.80*

	Geographic coverage	Horizontal Res	Measurement Range	Measure-ment Accuracy	Product measureme-nt precision
Cloud Height	Global	Resolution of IR Pixels	0-20km	0.5 km	1.5 km
Cloud Pressure	Global	Resolution of IR Pixels	100-1000 hPa	50 hPa	150 hPa

Cloud Temperature	Global	Resolution of IR Pixels	180-300 K	3 K	5 K

Furthermore, the GOES-R Series Ground Segment (GS) Project Functional and Performance Specification (F&PS) qualifies these requirements for cloudy regions with emissivities greater than 0.8.

3.2 Instrument Characteristics

The ACHA will operate on each pixel determined to be cloudy or probably cloud by the Cloud Mask. Table 2 summarizes the current channels used by the ACHA for the 16 modes it supports.

Table 2 *Wavelengths and associated modes for the ABI Cloud Height Algorithm (ACHA). Symbols (i,j,k,l,m,n,o,p) refer to channel indices.*

Wavelength (µm)	1	2	3	4	5	6	7	8	9	10	11	12	13	14	15	16
3.8		i														
6.2																i
6.7			i			i	i	i			i		i			j
7.3																k
8.5						j			i		j	i	j		i	l
10.4																m
11.2	i	j	j	i	i	k	j	j	j	i	k	j	k	i	j	n
12.3				j			k		k	j	l	k	l		k	o
13.3					j			k		k		l	m	j	l	p
13.6														k	m	
13.9														l	n	
14.2														m	o	

Table 3 *ACHA Modes Supported by Sensor. (* = default mode, += GOES-17 only)*

Sensor	Acha Modes Supported
AVHRR/1	1*
AVHRR/2	1,4*
AVHRR/3	1,4*
GOES I/M, MTSAT, COMS,FY-2	1,3,4,7*
GOES N/P	1,3,5,8*
GOES-R, AHI	1,2+,3,4,5,7,8,9,10*,12,13,16
MODIS	1,3,4,5,7,8,9,10*,12,13,14,15
MSG/SEVIRI	1,3,4,5,7,8,9,10*,12,13
VIIRS	1,4,9*
AVHRR+HIRS, VIIRS+CrIS	10*

In general, the ACHA relies on the infrared observations to avoid discontinuities associated with the transition from day to night. ACHA performance is sensitive to imagery artifacts and instrument noise.   Most important is our ability to accurately model the clear-sky values of the infrared absorption channels. The ability to perform the physical retrievals outlined in this document requires an accurate forward model, accurate ancillary data and well-characterized spectral response functions.

4 ALGORITHM DESCRIPTION

4.1 Algorithm Overview

The ACHA serves a critical role in the GOES-R ABI processing system. It provides a fundamental cloud property but also provides information needed by other cloud and non-cloud algorithms. As such, latency was a large concern in developing the ACHA. The current version of the ACHA algorithm draws on the following heritage algorithms:

- The CLAVR-x split-window cloud height from NESDIS, and
- The MODIS CO_2 cloud height algorithm developed by the UW/CIMSS.
- The GOES-R AWG 11/12/13.3 μm algorithm.

The ACHA derives the following cloud products (* = delivered as a cloud CDR to NCDC):
- Cloud-top temperature*,
- Cloud-top pressure*,
- Cloud-top height*, and
- Quality flags*,
- Cloud 11 μm emissivity,
- Cloud microphysical index (β),
- Cloud optical depth,
- Cloud particle size
- Lower cloud level temperature under overlapping condition
- Ice cloud fraction
- Cloud Type (modified by ACHA)

Section 3.4 describes the full set of outputs from the ACHA algorithm.

4.2 Processing Outline

The processing outline of the ACHA is summarized in Figure 1. The current ACHA is implemented with the NOAA/NESDIS/STAR GOES-R AIT processing framework (FRAMEWORK). FRAMEWORK routines are used to provide all of the observations and ancillary data to the algorithms. The ACHA is designed to run on segments of data where a segment consists of multiple scan lines.

19
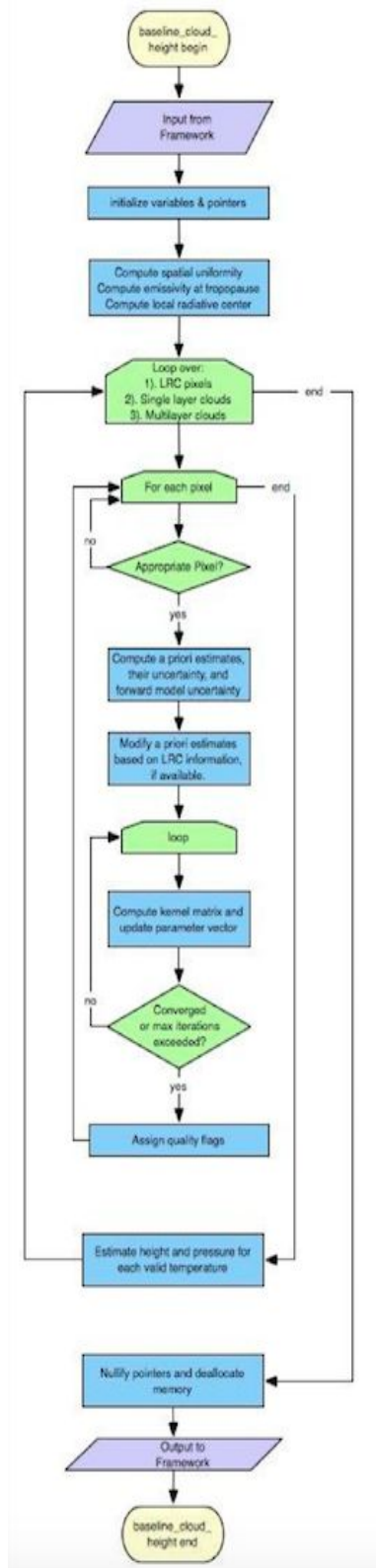
Figure 1 **High level flowchart of the ACHA illustrating the main processing sections.**

4.3 Algorithm Input

This section describes the input needed to process the ACHA. In its current configuration, the ACHA runs on segments comprising 200 scan lines. While this is the ideal number of scan-lines per segment the ACHA algorithm should be run on, the algorithm does benefit from running on a larger number of scan-lines. The ACHA must be run on arrays of pixels because spatial uniformity of the observations is necessary to the algorithm. In addition, the final algorithm design will include separate loops over those pixels in the segment determined to be local radiative centers (LRC), those pixels determined by the cloud typing algorithm to be single-layer clouds and those pixels determined to multi-layer clouds. The calculation of the LRC, which is done by the gradient filter, is described in the AIADD. The following sections describe the actual input needed to run the ACHA.

4.3.1 Primary Sensor Data

The list below contains the primary sensor data used by the ACHA. By primary sensor data, we mean information that is derived solely from the ABI observations and geolocation information. This description is for the ABI sensor, using the "baseline" mode and will necessarily change for the other imagers that ACHA supports.

- Calibrated radiances for channels 14 (11.2 μm).
- Calibrated brightness temperatures for channels 14 (11.2 μm), 15 (12.3 μm) and 16 (13.3 μm).
- Cosine of sensor viewing zenith angle.
- Satellite zenith angle.
- Space mask.
- Bad pixel mask for channels 14 (11.2 μm), 15 (12.3 μm), and 16 (13.3 μm).

4.3.2 Ancillary Data

The following lists the ancillary data required to run the ACHA. A more detailed description is provided in the AIADD. By ancillary data, we mean data that require information not included in the ABI observations or geolocation data.

- **Surface elevation**

- **Surface Type**

- **NWP level associated with the surface**

- **NWP level associated with the tropopause**

- **NWP tropopause temperature**

- **Profiles of height, pressure and temperature from the NWP**

- **Inversion level profile from NWP**

- **Surface temperature and pressure from NWP**

- **Viewing Zenith Angle bin**

- **NWP Line and element indices**

- **Clear-sky transmission, and radiance profiles for channels 14** (11.2 μm)**, 15** (12.3 μm) **and 16** (13.3 μm) **from the RTM**

- **Blackbody radiance profiles for channels 14** (11.2 μm)**, 15** (12.3 μm) **and 16** (13.3 μm) **from the RTM**

- **Clear-sky estimates of channel 14** (11.2 μm)**, 15** (12.3 μm) **and 16** (13.3 μm) **radiances from the RTM**

4.3.3 Derived Data

The following lists and briefly describes the data that are required by the ACHA that is provided by other algorithms.

- **Cloud Mask**
  A cloud mask is required to determine which pixels are cloudy or clear, which in turn determines which pixels are processed. This information is provided by the ABI Cloud Mask (ACM) algorithm. Details on the ACM are provided in the ACM ATBD.

- **Cloud Type/Phase**
  A cloud type and phase are required to determine which *a priori* information for the forward model are used. It is assumed that both the cloud type and phase are inputs to the ACHA algorithm. These products are provided by the ABI Cloud Type/Phase Algorithm. Information on the ABI Cloud Type/Phase is provided in the ABI Type/Phase ATBD.

- **Local Radiative Centers**
  Given channel 14 (11.2 μm) observed brightness temperatures, the local radiative center (LRC) is defined as the pixel location, in the direction of the gradient vector, upon which the gradient reverses. Practically, this starts with a 3 by 3 array surrounding a pixel, switches the center to the local maxima/minima in the array and initiates a new search. The gradient filter routine is required as an input

to the ACHA. The original method to compute the gradient function is described in Pavolonis (2009) and in the AIADD. Some changes have been made to be used in ACHA. The required inputs to the gradient filter are:

- o Calibrated brightness temperature at 11μm BT11,
- o The line and element size of the segment being processed,
- o The maximum search steps for local maxima/minima,
- o The upper and lower boundary values that the gradient must fall in between to initiate the search,
- o A flag for defining how the gradient reverses, i.e., when encountering a local maximum (1) or minimum (-1),
- o A binary mask for the segment of cloudy pixels that have non-missing BT11 for the segment,
- o The minimum and maximum valid BT11 values (220K and 290K respectively).

The outputs from the gradient filter are the line and element of the LRC.

- **Derived channel 14** (11.2 μm) **top of troposphere emissivity**
  The ACHA requires knowledge of the channel 14 emissivity of a cloud assuming that its top coincides with the tropopause. This calculation is done by using the measured channel 14 radiance, clear sky channel 14 radiance from the RTM, space mask, latitude/longitude cell index from the NWP, tropopause index from the NWP, viewing zenith angle bin index, and channel 14 μm blackbody radiance.

- **Standard deviation of the channel 14** (11.2 μm) **brightness temperature over a 3x3 pixel array.**

- **Standard deviation of the channel 14** (11.2 μm) **– channel 15** (12.3 μm) **brightness temperature difference over a 3x3 pixel array.**

- **Standard deviation of the channel 14** (11.2 μm) **– channel 16** (13.3 μm) **brightness temperature difference over a 3x3 pixel array.**

4.4 Theoretical Description

As described below, the ACHA represents an innovative approach that uses multiple IR channels within the algorithm that provides results that are consistent for all viewing conditions. This approach combines multiple window channel observations with single absorption channel observations to allow for the estimation of cloud height without large assumptions on cloud microphysics for the first time from a geostationary imager. The remainder of this section provides the physical basis for the chosen approach.

4.4.1 Physics of the Problem

The ACHA uses the infrared observations from the ABI to extract the desired information on cloud height. Infrared observations are impacted not only by the height of the cloud, but also its emissivity and how the emissivity varies with wavelength (a behavior that is tied to cloud microphysics). In addition, the emissions from the surface and the atmosphere can also be major contributors to the observed signal. Lastly, clouds often exhibit complex vertical structures that violate the assumptions of the single layer plane parallel models (leading to erroneous retrievals). The job of the ACHA is to exploit as much of the information provided by the ABI as possible with appropriate, computationally efficient and accurate methods to derive the various cloud height products.

4.4.1.1 Motivation for ACHA Channel Selection

The ACHA represents a merger of current operational cloud height algorithms run by NESDIS on the Polar Orbiting Environmental Satellite (POES) and GOES imagers. The current GOES-NOP cloud height algorithm applies the CO_2 slicing method to the 11 and 13.3 μm observations. This method is referred to as the CO_2/IRW approach. CO_2 slicing was developed to estimate cloud-top pressures using multiple channels typically within the 14 μm CO_2 absorption band. For example, the MODIS MOD06 algorithm (Menzel et al., 2006) employs four CO_2 bands, and the GOES Sounder approach also employs four bands. CO_2 slicing benefits from the microphysical simplicity provided by the spectral uniformity of the cloud emissivity across the 14 μm band. The GOES-NOP method suffers from two weaknesses relative to the MOD06 method. First, the assumption of spectral uniformity of cloud emissivity is not valid when applied to the 11 and 13.3 μm observations. Second, the 13.3 μm channel does not provide sufficient atmospheric opacity to provide the desired sensitivity to cloud height for optically thin high clouds (i.e., cirrus). For optically thick clouds, CO_2 slicing methods rely simply on the 11 μm observation for estimating the cloud height.

In contrast to the CO_2/IRW approach used for GOES-NOP, the method employed operationally for the POES imager (AVHRR) uses a split-window approach based on the 11 and 12 μm observations. Unlike the 13.3 μm band, the 11 and 12 μm bands are in spectral windows and offer little sensitivity to cloud height for optically thin cirrus. As described in Heidinger and Pavolonis (2009), the split-window approach does provide accurate measurements of cloud emissivity and its spectral variation.

Unlike the GOES-NOP imager or the POES imager, the ABI provides the 13.3 μm CO_2 channels coupled with multiple longwave IR windows (10.4, 11 and 12 μm). The ABI therefore provides an opportunity to combine the sensitivity to cloud height offered by a CO_2 channel with the sensitivity to cloud microphysics offered by window channels and to improve upon the performance of the cloud height products derived from the current operational imagers.

To demonstrate the benefits of the ACHA CO_2/Split-Window algorithm, the sensitivity to cloud pressure offered by the channels used in the ACHA was compared to other channel sets using co-located MODIS and CALIPSO observations. These results were taken from Heidinger et al. (2010). Figure 2 shows a false color image from AQUA/MODIS for a cirrus scene observed on August 10, 2006 over the Indian Ocean. The red line in Figure 2 shows the location of the CALIPSO track. This scene is characterized by a predominantly single cirrus cloud of varying optical thickness with thicker regions on the left-side of the figure. An image of the 532 nm CALIPSO data for the trajectory shown in Figure 2 is shown in Figure 3.
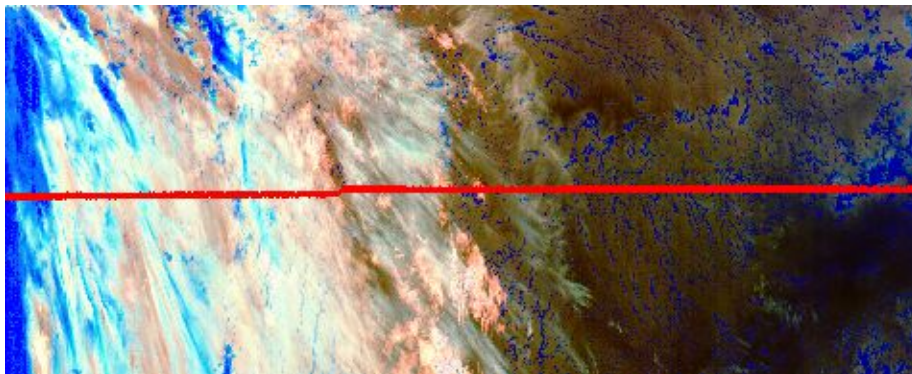
Figure 2 **A false color image constructed from 11 – 12µm BTD (Red), 4 – 11µm BTD (Green) and 11 µm BT reversed (Blue). Data are taken from AQUA/MODIS and CALIPSO/CALIOP on August 10, 2006 from 20:35 to 20:40 UTC. The red line is the CALIPSO track. In this color combination, cirrus clouds appear white but as the optical thickness increases, the ice clouds appear as light blue/cyan. Low-level water clouds appear as dark blue, and mid-level water clouds tend to have a red/orange color.**
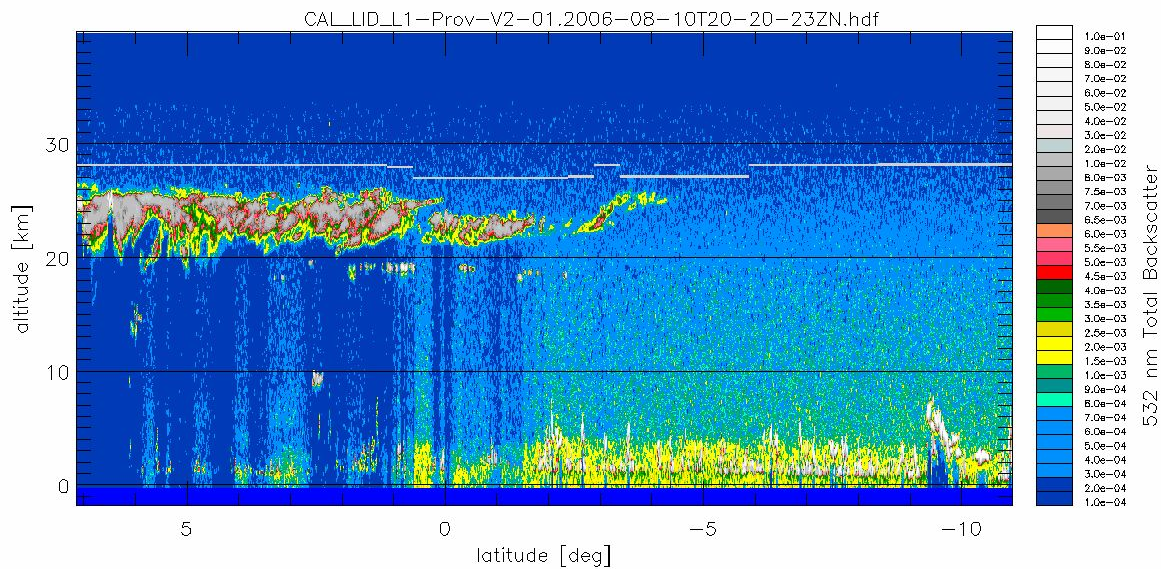
Figure 3 **The 532 nm total backscatter from CALIOP along the red line shown in Figure 2. The grey line in the centre image is the Tropopause.**

In the work of Heidinger et al. (2009), an analysis was applied to the above data to study the impact on the cloud-top pressure solution space offered by various channel combinations commonly used on operational imagers. The term solution space refers to the vertical region in the atmospheric column where a cloud can exist and match the observations of the channels used in the algorithm. As described in Heidinger et al. (2009) this analysis was accomplished specifically by computing the emissivity profiles for each channel and determining the levels at which the emissivities were all valid and where the spectral variation of the emissivities was consistent with the chosen scattering model. It is important to note that this analysis was not a comparison of algorithms, but a study of the impact of the pixel spectral information on the possible range of solutions.

Figure 4 shows the resulting computation of the cloud-top pressure solution space spanned by the ACHA CO_2/Split-Window algorithm (channels 14 (11.2 μm), 15 (12.3 μm) & 16 (13.3μm)). The grey area represents the region of the atmosphere where the MODIS observations of those channels were matched to within 0.5K. The blue points represent the cloud-top pressures where the cloud matched the MODIS observation most closely. In contrast, Figure 5 shows the same computation when using the VIIRS cloud-top height algorithm's channel set (8.5, 11.2 and 12.3 μm). As described by Heidinger et al. (2009), the large improvement in the sensitivity to cloud top pressure seen in ACHA versus the VIIRS algorithm is due to the presence of the CO_2 absorption channel. Because VIIRS offers only IR window channels, its ability to estimate the height of semi-transparent cirrus clouds with confidence is limited.
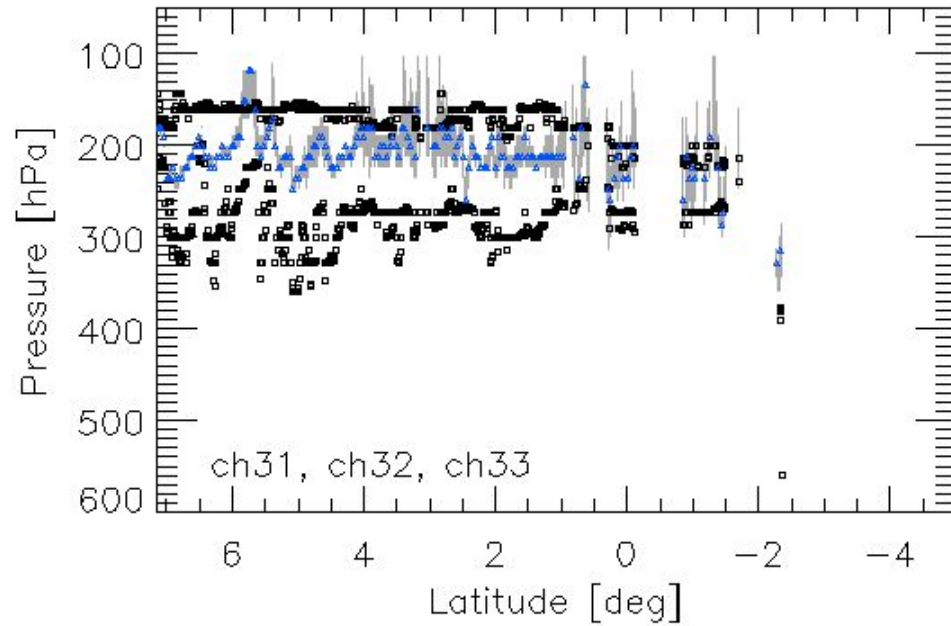
Figure 4 **Cloud-top pressure solution space provided by the ACHA channel set for the ice clouds along the CALIPSO track for August 10, 2006 20:35 – 20:40 UTC. The grey lines represent the solution space provided by the selected GOES-R ABI channels. The black symbols provide the CALIOP cloud boundaries for the highest cloud layer. The blue points represent the location of the optimal cloud-top pressure solutions with this channel set. Note that channel numbers in this figure correspond to the MODIS sensor. For clarity, only every fifth optimal cloud-top pressure solution is plotted.**
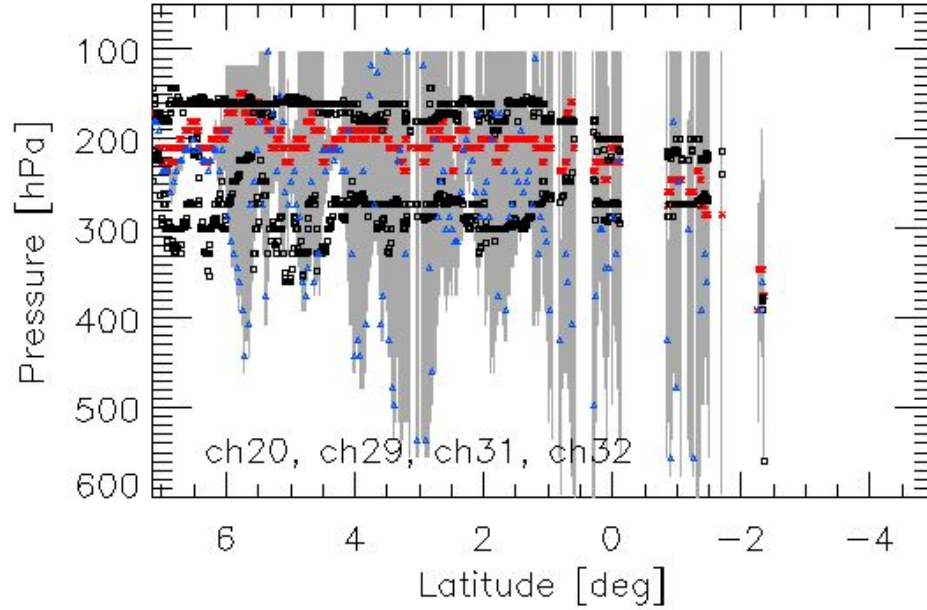
Figure 5 **Same as** Figure 4 **computed for the VIIRS channel set (3.75, 8.5, 11 and 12 μm). Red points show the MODIS (MYD06) results for reference. Same as** Figure 4**, channel numbers in this figure correspond to the MODIS sensor.**

4.4.1.2 Radiative Transfer Equation

The radiative transfer equation (1) employed here is given as

$$R_{obs} = e_c R_{ac} + t_{ac} e_c B(T_c) + R_{clr}(1 - e_c) \quad \text{(Eq. 1)}$$

where R_{obs} is the observed top-of-atmosphere radiance, T_c is the cloud temperature, B() represents the Planck Function and R_{clr} is the clear-sky radiance (both measured at the top of the atmosphere). R_{clr} is expressed as $e_s B(T_s)t_{all} + R_{atm}$, where e_s is surface emissivity, T_s is surface temperature or lower cloud layer temperature depending whether multilayer cloud is detected, t_{all} is total atmospheric transmission, and R_{atm} is total upward atmospheric emission. R_{ac} is the above-cloud emission; t_{ac} is the above-cloud transmission along the path from the satellite sensor to the cloud pixel. Finally, the cloud emissivity is represented by e_c. All quantities in Eq. 1 are a function of wavelength, λ, and are computed separately for each channel.

As described later, the 11 μm cloud emissivity is directly retrieved by the ACHA. The 12 and 13.3 μm cloud emissivities are not retrieved but they are utilized during the retrieval process.

To account for the variation of e_c with each channel, the β parameter is evoked. For any two-channel pair (1,2), the value of β can be constructed using the following relationship:

$$\beta_{1,2} = \frac{ln(1-e_2)}{ln(1-e_1)} \qquad \text{(Eq. 2)}$$

Using this relationship, the cloud emissivities at 12 and 13 um can be derived from the cloud emissivity value at 11 μm as follows:

$$e_c(12\mu m) = 1 - [1 - e_c(11\mu m)]^{\beta(12/11\mu m)} \qquad \text{(Eq. 3)}$$

$$e_c(13.3\mu m) = 1 - [1 - e_c(11\mu m)]^{\beta(13.3/11\mu m)} \qquad \text{(Eq. 4)}$$

For the remainder of this document, the value of e_c will refer to the cloud emissivity at 11 μm and β will refer to the β (11/12μm) value unless stated otherwise. β is a convenient parameter because it also provides a direct link to cloud microphysics which is discussed in the next section.

While the above radiative transfer equation is simple in that it assumes no scattering and that the cloud can be treated as a single layer, it does allow for semi-analytic derivations of the observations to the controlling parameters (i.e., cloud temperature). This behavior is critical because it allows for an efficient retrieval without the need for large lookup tables.

4.4.1.3 Cloud Microphysical Assumptions

One of the strengths of the ACHA is that it allows cloud microphysics to vary during the retrieval process which should improve the cloud height estimates (Heidinger et al., 2009). Cloud microphysics is included in the retrieval through the spectral variation of the β parameters. The variation of β between different channel pairs is a function of particle size and ice crystal habit. For example, Parol et al. (1991) showed that β can be related to the scattering properties using the following relationship where ω is the single scattering albedo, g is the asymmetry parameter and σ_{ext} is the extinction coefficient:

$$\beta_{2,1} = \frac{[1-\omega(\lambda_1)g(\lambda_1)]\sigma_{ext}(\lambda_1)}{[1-\omega(\lambda_2)g(\lambda_2)]\sigma_{ext}(\lambda_2)} \qquad \text{(Eq. 5)}$$

This relationship between β and the scattering properties will allow the ACHA to estimate cloud particle size from the retrieved β values.

While the scattering properties for water clouds are well modeled by Mie theory, the scattering properties of ice clouds are more uncertain. To define a relationship between the β values for ice clouds, assumptions have to be made about the ice crystals. In the ACHA, we use the ice scattering models provided by Professor Ping Yang at Texas A&M University (Yang et al., 2013). In this database, ice models are separated by habits. To help pick a habit, β values were computed using CALIPSO Imaging Infrared Radiometer (IIR) effective emissivity products. We then compared how the observed β values corresponded with those computed from the scattering. The results in Figure 6 indicated that the aggregate column and the two-habit model, which is based on both a single hexagonal column and hexagonal aggregates, modeled the observed data the best. Note that in this figure the β relationship between different channel pairs are assumed to be linear. For water clouds, standard Mie theory computed scattering properties are used to predict the β values and their relationship with each other.
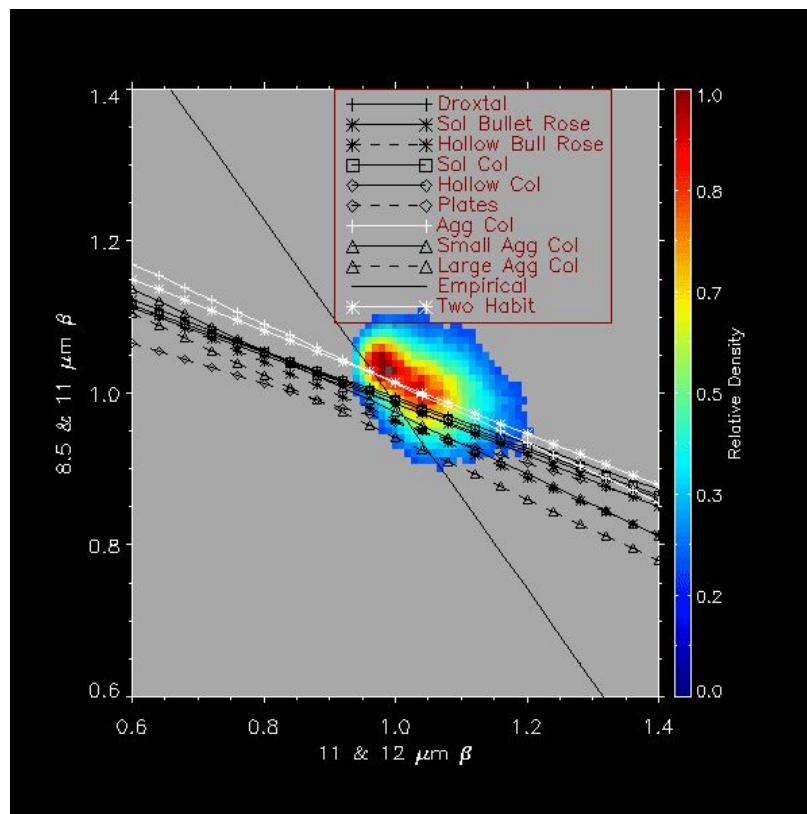
Figure 6 **Comparison of the variation of β values for 11 and 12 μm against those for 11 and 8.5 μm. The cloud of points represents those computed using CALIPSO observations between January 1 and 19 in 2013. The lines except the Empirical one represent predictions directly based on the Yang et. al (2013) scattering database.**

It is mentioned above that β is a function of particle size and habit. Hence, effective particle size can be estimated once β is known with ice crystal habit assumed. However, it is found that particle size can vary significantly using β from different channel pairs

and fixed habit. Therefore, a new empirical model based on radiometric consistent particle size is derived, without assuming a fixed habit (Heidinger et al. 2015). Figure 7 shows the computed variation of the 11 and 12 μm β with the 11 and 13.3 μm β and Figure 8 shows the variation of the 11 and 12 μm β with particle size. There is a distinct change of the empirical model β curve compared to aggregates. The empirical model is also effective in reducing the retrieved cloud height and the validation against CALIPSO is better (Figure 9). In implementation a physically based ice crystal habit is preferred in retrieving ice cloud height. After careful comparison, it is found that using the single scattering properties (Yang et al. 2013) computed for the two habit model show best consistency with the empirical model. Therefore, this habit is currently used to produce NOAA VIIRS cloud height products in the optimal estimation approach described in the next session.

For a given pixel, β is computed using ice fraction as weighting and values from both water and ice phases as follows:

$$\beta = (1 - f_{ice})\beta_{water} + f_{ice}\beta_{ice} \qquad (\text{Eq. 6})$$

where f_{ice} is ice fraction.
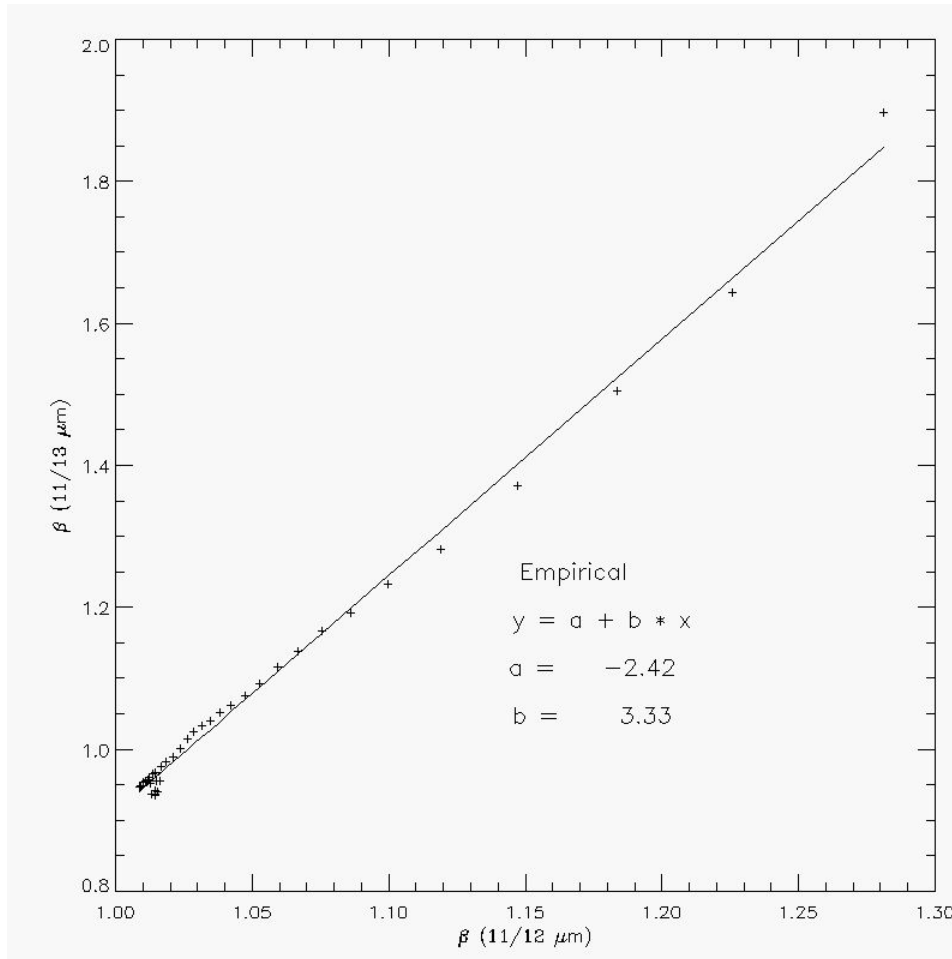
Figure 7 **Computed variation and linear-fit of the 11 and 13.3 μm β values to those computed using 11 and 12 μm. β is a fundamental measure of the spectral variation of cloud emissivity, and this curve is used in the forward model in the retrieval. The data shown are based on a radiometric consistent empirical model. For water clouds, Mie theory predicts a = -0.728 and b = 1.743.**
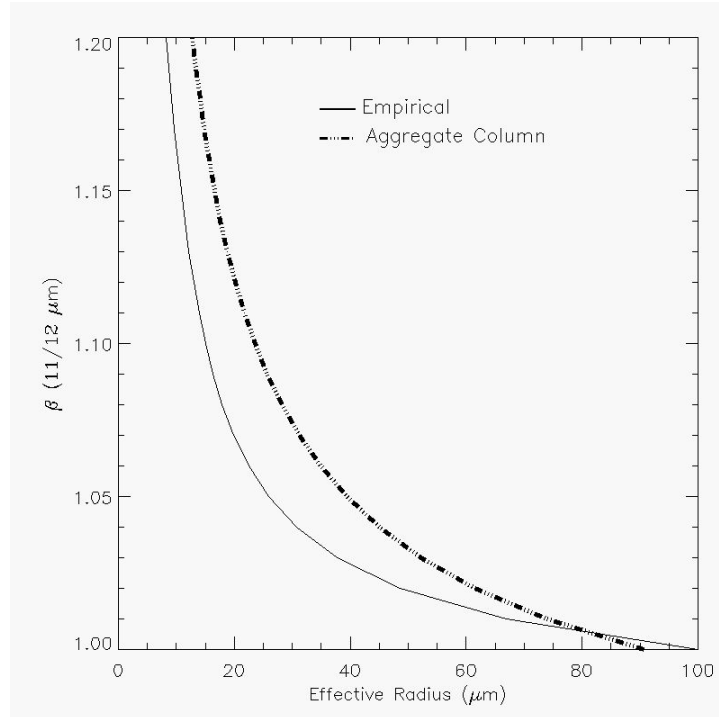
Figure 8 **Variation of the 11 and 12 μm β values as a function of the ice crystal radius for both the Empirical model and Aggregate Column model. This relationship is used in the infrared retrieval to produce an estimation of cloud particle size from the final retrieved β values.**
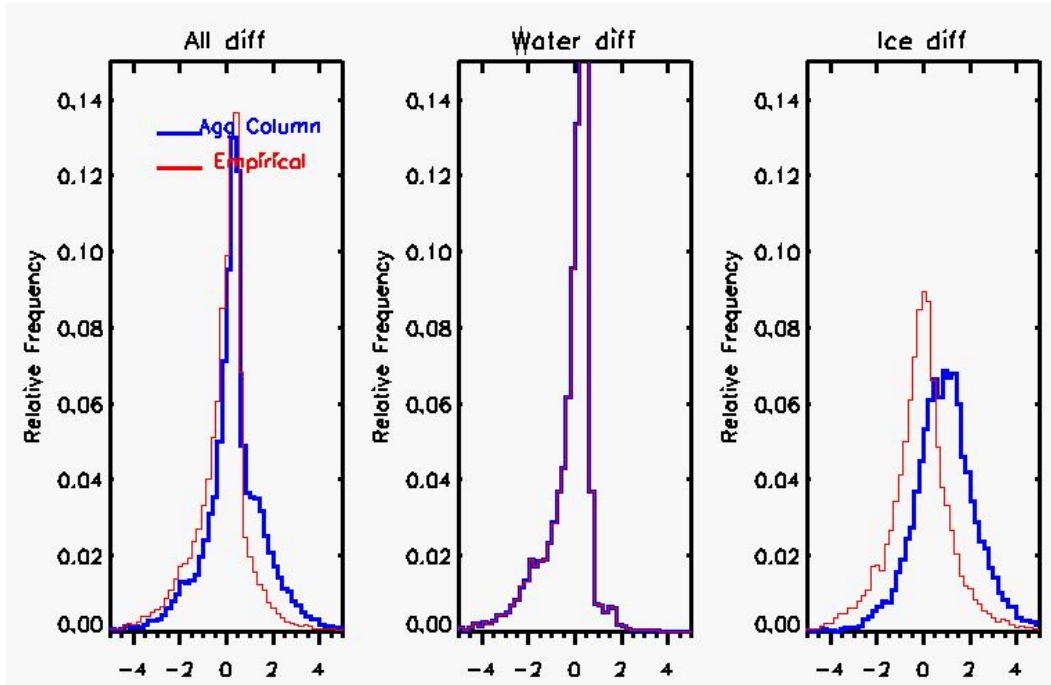
Figure 9 **Histogram showing differences between ACHA and CALIPSO cloud top height, using two ice models. One day of MODIS 5km data (06/30/2010) are run to simulate VIIRS output. Note that the CALIPSO cloud top heights shown here are adjusted to simulate IR retrieval and tend to report lower values compared to the true top.**

4.4.2 Mathematical Description

The mathematical approach employed here is the optimal estimation approach described by Rodgers (1976). The optimal estimation approach is also often referred to as a 1DVAR approach. The benefits of this approach are that it is flexible and allows for the easy addition or subtraction of new observations or retrieved parameters. Another benefit of this approach is that it generates automatic estimates of the retrieval errors. The following description of the method employs the same notation as Rodgers (1976) but provides only a brief review.

The optimal estimation approach minimizes a cost function, Φ, given by

$$\phi = (x - x_a)^T S_a^{-1} (x - x_a) + (y - f(x))^T S_y^{-1} (y - f(x)) \quad \text{(Eq. 7)}$$

where **x** is a vector of retrieved parameters, **x$_a$** is a vector housing the *a priori* values of **x** (which also serve as a first guess to begin iterations to a convergent solution), **y** is the vector of observations, and **f** is the forward model's estimates of the values of **y** under the assumptions of state **x**. **S$_a$** is the error covariance matrix corresponding to the values of **x$_a$**, and **S$_y$** is the error covariance matrix for the forward model and measurements.

In each retrieval iteration, the state vector **x** is incremented as follows:

$$\delta x = S_x[K^T S_y^{-1}(y - f(x)) + S_a^{-1}(x_a - x)] \qquad \text{(Eq. 8)}$$

where **K** is the Jacobian or Kernel matrix (whose computation is described below) and $\mathbf{S_x}$ is the covariance error matrix of **x** which is computed as

$$S_x = (S_a^{-1} + K^T S_y^{-1} K)^{-1}. \quad \text{(Eq. 9)}$$

The retrieval iterations are conducted until the following criterion is met:

$$\left| \sum \delta x S_x^{-1} \delta x \right| \leq \frac{p}{2} \qquad \text{(Eq. 10)}$$

where **p** is the number of elements in **x**.

In ACHA, the **y** and **x** vectors are defined as follows.

$$y = \begin{pmatrix} BT(11\mu m) \\ BTD(11-12\mu m) \\ BTD(11-13.3\mu m) \end{pmatrix} \quad \text{(Eq. 11)}$$

$$x = \begin{pmatrix} T_c \\ e(11\mu m) \\ \beta(12/11um) \\ T_s \\ f_{ice} \end{pmatrix} \qquad \text{(Eq. 12)}$$

$$x_a = \begin{pmatrix} T_{c\_ap} \\ e(11\mu m)\_ap \\ \beta(12/11\mu m)\_ap \\ T_{s\_ap} \\ f_{ice\_ap} \end{pmatrix} \qquad \text{(Eq. 13)}$$

The Kernel matrix contains the partial derivatives of each element of **f(x)** to each element of **x**. In Heidinger and Pavolonis (2009), the equations defining all of the elements of **K** except those that involve the 13.3 μm channel are given. The following relationships

repeat those in Heidinger and Pavolonis (2009) and provide the remaining terms used in the ACHA.

4.4.2.1 ACHA Mode 10 Mathematical Description

$$K$$
$$= \begin{bmatrix} \dfrac{\partial BT(11\mu m)}{\partial T_c} & \dfrac{\partial BT(11\mu m)}{\partial e(11\mu m)} & \dfrac{\partial BT(11\mu m)}{\partial \beta(12/11\mu m)} & \dfrac{\partial BT(11\mu m)}{\partial T_s} & \dfrac{\partial BT(11\mu m)}{\partial f_{ice}} \\ \dfrac{\partial BTD(11-12\mu m)}{\partial T_c} & \dfrac{\partial BTD(11-12\mu m)}{\partial e(11\mu m)} & \dfrac{\partial BTD(11-12\mu m)}{\partial \beta(12/11\mu m)} & \dfrac{\partial BTD(11-12\mu m)}{\partial T_s} & \dfrac{\partial BTD(11-12\mu m)}{\partial f_{ice}} \\ \dfrac{\partial BTD(11-13.3\mu m)}{\partial T_c} & \dfrac{\partial BTD(11-13.3\mu m)}{\partial e(11\mu m)} & \dfrac{\partial BTD(11-13.3\mu m)}{\partial \beta(12/11\mu m)} & \dfrac{\partial BT(11-13.3\mu m)}{\partial T_s} & \dfrac{\partial BTD(11-13.3\mu m)}{\partial f_{ice}} \end{bmatrix}$$

(Eq. 14)

The expressions required for the first column of **K** are given by Eqs. 14-16.

$$\frac{\partial BT(11\mu m)}{\partial T_c} = e_c(11\mu m)t_{ac}(11\mu m)\left(\frac{\partial B(11\mu m)}{\partial T_c}\right)\left(\frac{\partial B(11\mu m)}{\partial T}\right)^{-1} \quad \text{(Eq. 15)}$$

$$\frac{\partial BTD(11-12\mu m)}{\partial T_c} = \frac{\partial BT(11\mu m)}{\partial T_c} - e_c(12\mu m)t_{ac}(12\mu m)\left(\frac{\partial B(12\mu m)}{\partial T_c}\right)\left(\frac{\partial B(12\mu m)}{\partial T}\right)^{-1} \quad \text{(Eq. 16)}$$

$$\frac{\partial BTD(11-13.3\mu m)}{\partial T_c} =$$
$$\frac{\partial BT(11\mu m)}{\partial T_c} - e_c(13.3\mu m)t_{ac}(13.3\mu m)\left(\frac{\partial B(13.3\mu m)}{\partial T_c}\right)\left(\frac{\partial B(13.3\mu m)}{\partial T}\right)^{-1} \quad \text{(Eq. 17)}$$

The expressions for the second column of **K** are given by Eqs. 18-20.

$$\frac{\partial BT(11\mu m)}{\partial e_c(11\mu m)} = [R_{cld}(11\mu m) - R_{clr}(11\mu m)](\frac{\partial B(11\mu m)}{\partial T})^{-1}$$
(Eq. 18)

$$\frac{\partial BTD(11-12\mu m)}{\partial e_c(11\mu m)} = \frac{\partial BT(11\mu m)}{\partial e_c(11\mu m)} - [R_{cld}(12\mu m) - R_{clr}(12\mu m)]\left[\beta(12/11\mu m)(1-e_c(11\mu m))^{\beta(12/11\mu m)-1}\right] * (\frac{\partial B(12\mu m)}{\partial T})$$

(Eq. 19)

$$\frac{\partial BTD(11-13.3\mu m)}{\partial e_c(11\mu m)} = \frac{\partial BT(11\mu m)}{\partial e_c(11\mu m)} - \left[R_{cld}(13.3\mu m) - R_{clr}(13.3\mu m)\right]\left[\beta(13.3/11\mu m)(1-e_c(11\mu m))^{\beta(13.3/11\mu m)-1}\right] * ($$

(Eq. 20)

The derivative of each forward model simulation with respect to $\beta(12/11\mu m)$ is given by the following equations:

$$\frac{\partial BT(11\mu m)}{\partial \beta(12/11\mu m)} = 0.0$$ (Eq. 21)

$$\frac{\partial BTD(11-12\mu m)}{\partial \beta(12/11\mu m)} = \left[R_{cld}(12\mu m) - R_{clr}(12\mu m)\right] ln\left[1 - e_c(11\mu m)\right] * \left[1 - e_c(12\mu m)\right](\frac{\partial B(12\mu m)}{\partial T})^{-1}$$

(Eq. 22)

$$\frac{\partial BTD(11-13.3\mu m)}{\partial \beta(12/11\mu m)} = \left[R_{cld}(13.3\mu m) - R_{clr}(13.3\mu m)\right] ln\left[1 - e_c(11\mu m)\right] * \left[1 - e_c(13.3\mu m)\right](\frac{\partial \beta(13.3/11\mu m)}{\partial \beta(12/11\mu m)})(\frac{\partial B(13.3\mu m)}{\partial T}$$
(Eq. 23)

The values of $\frac{\partial \beta_{11/13}}{\partial \beta_{11/12}}$ are computed using the regression shown in Figure 7. For water clouds, the same form of a regression shown in Figure 7 is used except that the a-coefficient is -0.728 and the b-coefficient is 1.743.

The derivative with respect to T_s is given as:

$$\frac{\partial BT(11\mu m)}{\partial Ts} = t_{all} e_s(11\mu m)(\frac{\partial B(11\mu m)}{\partial T_s})\left(\frac{\partial B(11\mu m)}{\partial T}\right)^{-1}(1-e_c(11\mu m))$$

(Eq. 24)

$$\frac{\partial BTD(11-12\mu m)}{\partial T_s} = \frac{\partial BT(11\mu m)}{\partial T_s} - \left(\frac{\partial B(12\mu m)}{\partial T}\right)^{-1}\frac{\partial B(12\mu m)}{\partial T_s}(1-e_c(12\mu m))e_s(12\mu m)t_{all}(12\mu m)$$
(Eq. 25)

$$\frac{\partial BTD(11-13.3\mu m)}{\partial T_s} = \frac{\partial BT(11\mu m)}{\partial T_s} - \left(\frac{\partial B(13.3\mu m)}{\partial T}\right)^{-1}\frac{\partial B(13.3\mu m)}{\partial T_s}(1-e_c(13.3\mu m))e_s(13.3\mu m)t_{all}(13.3\mu m)$$
(Eq. 26)

Finally, the derivatives with respect to f_{ice} is as follows:

$$\frac{\partial BT(11\mu m)}{\partial f_{ice}} = 0 \qquad (\text{Eq. } 27)$$

$$\frac{\partial BTD(11-12\mu m)}{\partial f_{ice}} = \frac{\partial BTD(11-12\mu m)}{\partial \beta(12/11um)} \frac{\partial \beta(12/11um)}{\partial f_{ice}} \qquad (\text{Eq. } 28)$$

where $\frac{\partial \beta(12/11um)}{\partial f_{ice}} = \beta_{ice} - \beta_{water}$

$$\frac{\partial BTD(11-133\mu m)}{\partial f_{ice}} = \frac{\partial BTD(11-133\mu m)}{\partial \beta(12/11um)} \frac{\partial \beta(12/11um)}{\partial f_{ice}} \qquad (\text{Eq. } 29)$$

4.4.2.2 Estimation of Prior Values and their Uncertainty

The proper implementation of ACHA requires meaningful estimates of *a priori* values housed in x_a and their uncertainties housed in S_a. S_a is a two-dimensional matrix with each dimension being the size of x_a. For the ACHA, we assume S_a is a diagonal matrix with each element being the assumed variance of each element of x_a as illustrated below.

$$S_a = \begin{pmatrix} \sigma^2_{Tc\_ap} & 0 & 0 & 0 & 0 \\ 0 & \sigma^2_{e(11\mu m)\_ap} & 0 & 0 & 0 \\ 0 & 0 & \sigma^2_{\beta(12/11\mu m)\_ap} & 0 & 0 \\ 0 & 0 & 0 & \sigma^2_{Ts\_ap} & 0 \\ 0 & 0 & 0 & 0 & \sigma^2_{fice\_ap} \end{pmatrix} \qquad (\text{Eq. } 30)$$

In the ACHA, we currently use the *a priori* estimate of x_a and S_a based on phase and 11μm properties, as well as from calipso values as reported by Heidinger and Pavolonis (2009). For water typed clouds, the *a priori* values of Tc use the opaque level temperature at the LRC, and emissivities are computed from an *a priori* estimate of optical thickness and satellite zenith angle:

$$\varepsilon c\_ap(water) = 1.0 - \exp(-\tau\_ap\_water / mu) \qquad (\text{Eq. } 31)$$

where a value of 3.0 is use for $\tau\_ap(water)$, and *mu* is the cosine of the satellite zenith angle. Fixed values of 10 K and 0.2 are used for the values of σ^2.

For ice type clouds, the *a priori* values and σ^2 of T_c and emissivity are computed as follows:

$$Tc\_ap(ice) = \begin{cases} Tc\_opaque, \text{ if } \varepsilon c11\_tropo > 0.95 \\ Tc\_cirrus, \text{ if } ec11\_tropo < 0.5 \\ \varepsilon c11\_tropo * Tc\_opaque\_LRC + (1.0 - \varepsilon c11\_tropo) * (Tc\_cirrus), \text{ if othersise} \end{cases}$$

$$\sigma^2(Tc)\_ap(ice) = \begin{cases} Tc\_uncer\_opaque, \text{ if } \varepsilon c11\_tropo > 0.95 \\ Tc\_uncer\_cirrus, \text{ if } ec11\_tropo < 0.5 \\ \varepsilon c11\_tropo * Tc\_uncer\_opaque + (1.0 - \varepsilon c11\_tropo) * Tc\_uncer\_cirrus, \text{ if othersise} \end{cases}$$

$$\varepsilon c\_ap(ice) = \varepsilon c11\_tropo$$

$$\sigma^2(\varepsilon c)\_ap(ice) = 0.4$$

(Eq. 32)

where $\varepsilon c11\_tropo$ is the 11 μm emissivity at tropopause, *Tc_cirrus* is the *a priori* value for cirrus cloud temperature from a lookup table, and the values for *Tc_uncer_opaque*, *Tc_uncer_cirrus* are 10K, 20K.

The *a priori* values of β are taken from scattering theory and are set to 1.06 for ice-phase clouds and 1.3 for water-phase clouds. The standard deviation of β is assumed to be 0.2 based on the distributions of Heidinger and Pavolonis (2009).

If a multilayer cloud is not detected, the NWP surface temperature is used as the *a priori* for Ts. Under multilayer situations, the *a priori* is the smoothed value of mean nearby water cloud temperatures if available, and the value of surface temperature minus a predefined offset (currently 10K) if not. The uncertainty is set as 1K and 20K, respectively, for single and multilayer conditions.

Table 4 provides the current a priori and uncertainty values used in ACHA.

Table 4 *The* a priori *(first guess) retrieval values used in the ACHA retrieval.*

Cloud Type	T_c	$\sigma^2(T_c)$	ε	$\sigma^2(\varepsilon)$	β	$\sigma^2(\beta)$
Fog	T_{opaque}_LRC	10 K	$\varepsilon c\_ap(water)$	0.2	1.3	0.2
Water	T_{opaque}_LRC	10 K	$\varepsilon c\_ap(water)$	0.2	1.3	0.2
Supercooled	T_{opaque}_LRC	10 K	$\varepsilon c\_ap(water)$	0.2	1.3	0.2
Mixed	T_{opaque}_LRC	10 K	$\varepsilon c\_ap(water)$	0.2	1.3	0.2
Thick Ice	Tc_ap(ice)	$\sigma^2(Tc)\_ap(ice)$	$\varepsilon c\_ap(ice)$	0.4	1.06	0.2
Cirrus	Tc_ap(ice)	$\sigma^2(Tc)\_ap(ice)$	$\varepsilon c\_ap(ice)$	0.4	1.06	0.2
Multi-layer	Tc_ap(ice)	$\sigma^2(Tc)\_ap(ice)$	$\varepsilon c\_ap(ice)$	0.4	1.06	0.2

4.4.2.3 Estimation of Forward Model Uncertainty

This section describes the estimation of the elements of S_y which contain the uncertainty expressed as a variance of the forward model estimates. S_y is assumed to be a symmetric matrix. Both diagonal and off-diagonal components are computed.

Assumed to be symmetric, S_y can be expressed as follows:

$$S_y = \begin{pmatrix} \sigma^2_{BT(11\mu m)} & \sigma^2_{cov\,BT(11,12\mu m)} & \sigma^2_{cov\,BT(11,13\mu m)} \\ \sigma^2_{cov\,BT(11,12\mu m)} & \sigma^2_{BTD(11-12\mu m)} & \sigma^2_{cov\,BT(12,13\mu m)} \\ \sigma^2_{cov\,BT(11,13\mu m)} & \sigma^2_{cov\,BT(1213\mu m)} & \sigma^2_{BTD(11-133\mu m)} \end{pmatrix} \quad \text{(Eq. 33)}$$

The diagonal variance terms are computed by summing up three components:

$$\sigma^2_{diag} = \sigma^2_{instr} + [1 - e_c(11\mu m)]^2 \sigma^2_{clr} + \sigma^2_{hetero} \quad \text{(Eq. 34)}$$

The first component (σ^2_{instr}) represents instrument noise and calibration uncertainties. The second component represents uncertainties caused by the clear-sky radiative transfer (σ_{clear}). σ_{clear} is assumed to decrease linearly with increasing e_c. For opaque clouds, the uncertainties associated with clear-sky radiative transfer are assumed to be negligible. Due to the large variation in NWP biases on land and ocean, separate land and ocean uncertainties are assumed. The third component (σ_{hetero}) is the term that accounts for the larger uncertainty of the forward model in regions of large spatial heterogeneity. Currently, the ACHA uses the standard deviation of each element of y computed over a 3x3 pixel array as the value of σ_{hetero}. The off diagonal variance terms are expressed in a simpler way:

$$\sigma^2_{off-diag} = [1 - e_c(11\mu m)]^2 \sigma^2_{clr}(11,12/13\mu m) \quad \text{(Eq. 35)}$$

4.4.2.4 Estimation of Quality Flags and Errors

One of the benefits of the 1DVAR approach is the diagnostic terms it generates automatically. If the values of S_a, S_y and K are properly constructed, the values of S_x should provide an estimate of the uncertainties of the retrieved parameters, x. The diagonal term of S_x provides the uncertainty expressed as a variance of each parameter. While these estimates are useful, the current ACHA also generates a 4-level quality flag. The integer quality flags are determined by the relative values of the diagonal terms of S_x and S_a. If the estimated uncertainty in an element of x is less than one third of the

prescribed uncertainty of the corresponding element of x_a, a parameter quality indicator, which is not the product quality flag described in section 3.4.3.3, of 3 is assigned. Similarly a parameter quality indicator of 2 is assigned for pixels where the estimated uncertainty of x lies between one third and two thirds of the uncertainty of the corresponding element of x_a. Values with higher uncertainties are given a parameter quality indicator of 1.   Retrievals that do not converge are given a parameter quality indicator of 0. A description of the parameter quality indicator is in section 3.4.3.2.

4.4.2.5 Impact of Local Radiative Center Pixels

As discussed above, the first pass through the retrieval occurs for those pixels determined to be local radiative centers which physically correspond to local maxima in cloud opacity. The full pixel processing order is described below. The objective is to first apply the retrieval to the more opaque pixels and to use this information for the less opaque pixels. In the ACHA, the *a priori* value of T_c for pixels that have local radiative centers identified for them are assumed to be the values of T_c estimated for the local radiative centers. The uncertainty values of the forward model remain those given in Table 5.

Table 5 *Values of uncertainty for the forward model used in the ACHA retrieval.*

Element of f	σ_{instr}	σ_{clear} (Ocean)	σ_{clear} (Land)
T(11um)	1.0	1.5	5.0
BTD(11 – 12μm)	1.0	0.5	1.0
BTD(11 – 13μm)	2.0	4.0	4.0

4.4.2.6 Treatment of Multi-layer Clouds

For pixels determined to be multi-layer clouds, the lower boundary condition is assumed to be a lower cloud and not the surface of the earth. With this assumption, the forward model remains unchanged when treating multi-layer clouds. The same equations apply except that the clear-sky observations are recomputed to reflect the change in the lower boundary condition.

As of Version 3.1 of this document, the temperature/height of the lower clouds layer is dynamically computed from the optimal estimation algorithm. In the ACHA, the *a priori* values for the lower cloud Tc is estimated using information about the height of nearby single layer low clouds using the KD-tree technique. Currently, three predictors including latitude, longitude and cloud type are used in the KD-tree method to make predictions from single layer water cloud retrievals for the lower cloud a-priori value. Figure 10 provides a visual aid for understanding this process. In this example, assume that the ABI pixel observed above Low Cloud #3 is correctly identified as a multi-layer cloud by the ABI cloud typing algorithm. Also, assume that Low Clouds #1 and #5 are correctly identified as low clouds and have successful cloud height solutions from the ACHA.   The ACHA uses the height information for Low Clouds #1 and #5 to estimate the height of Low Cloud #3 instead of assuming a fixed height of all low clouds detected

40
below high clouds. In the actual application, the KD-tree method does not necessarily require the source pixels (Low Clouds #1 and #5) close to the target pixels (Low Cloud #3). However, the number of source pixels within a segment needs to be greater than a threshold to apply KD-tree, and it is set as 10 currently. When this threshold is not met, this computation is accomplished by taking the mean of all low cloud pressures that surround the multi-layer cloud pixel within a NxN box. The size of the box (N) varies with the sensor resolution. If no low cloud results are found within the NxN box, a default value of the cloud temperature is used. This default value is 10K lower than the surface temperature. The application of this logic requires that the low cloud information be available before processing the multi-layer pixels. This logic is described in the next section.
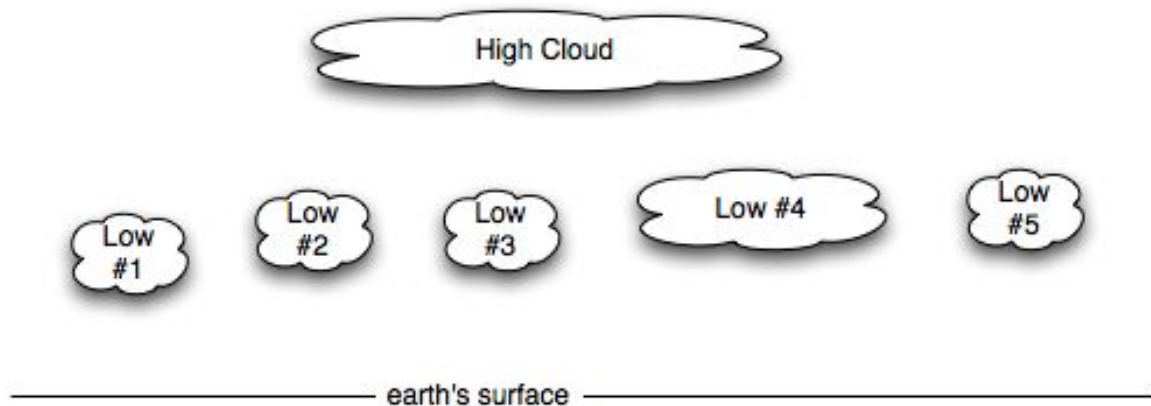
Figure 10 **Schematic illustration of multi-layer clouds.**

4.4.2.7 Pixel Processing Order with the ACHA

As stated above, applying the multi-layer logic and applying local-radiative center logic require that some pixels be processed before others. In this section, we describe this logic. The pixel processing order in the ACHA is as follows:
1. Single-layer Radiative Centers,
2. Non-local radiative center water clouds,
3. Multi-layer clouds, and
4. All remaining unprocessed cloudy pixels.
5. Redo all thin cirrus clouds using a-priori temperature derived from thicker ice clouds, if the use_cirrus_flag is set as on

Pixels that are single-layer radiative centers can be done first since they rely not on the results of other pixels. Pixels that are single-layer water clouds can then be processed because they would be influenced by the pixels that are single layers and radiative

centers. Single-layer ice pixels cannot be processed yet since they may require knowledge of the multi-layer results if their LRC computation points to a multi-layer pixel. The next pixels that can be processed are the multi-layer pixels. After this computation, all remaining pixels can be processed.

Cirrus clouds are commonly originated from deep convective clouds that extend horizontally to larger areas, thus it is reasonable to assume cirrus having similar temperature as nearby thicker ice cloud tops. An ACHA parameter "use_cirrus_flag" allows users to redo thin cirrus cloud retrieval using a-priori temperature derived from nearby thicker ice clouds. Similarly, the KD-tree method is utilized to derive the cirrus a-priori, and currently, three predictive variables — latitude, longitude, and cloud type — are used for this purpose. The use of KD-tree has the advantage of providing better and smooth spatial features compared to a simple neighbor averaging method.

4.4.2.8 Computation of Cloud Height and Cloud Pressure

Once T_c is computed, the NWP temperature profiles are used to interpolate the values of cloud-top pressure, P_c, and cloud-top height, Z_c. Two separate methods are applied depending on whether the cloud is within an inversion or not. An inversion is defined as a region in the atmosphere where the temperature increases with height. Figure 11 provides an illustration of an inversion. When a cloud temperature is found to reside outside of an inversion, a simple linear interpolation is used to estimate cloud-top pressure and height. In the presence of inversions, the monotonic relationship between temperature and pressure/height disappears and a single value of cloud temperature can correspond to multiple pressure or height values. Atmospheric inversions are common at low levels over the ocean and over cold polar surfaces. This issue plagues all infrared cloud height algorithms including those employed by the MODIS and GOES sounder teams.

The presence of low-level inversions is determined by analysis of the NWP temperature profile. If any layer below 600 hPa is found to be warmer than the layer below it, the clouds are assumed to reside in an inversion as illustrated in Figure 11. The vertical resolution of NWP profiles is not sufficient to use them directly in the presence of inversions. In implementation, low level inversion is detected by comparing the difference (DeltaT) between the cloud temperature and the surface temperature and a preselected threshold. If smaller, the cloud height is estimated by dividing DeltaT by a predefined lapse rate. Currently, the lapse rate is determined by both the cloud temperature and surface temperature from a lookup table computed using calipso observations. This procedure was initially implemented for water-phase clouds over water surfaces and then extended to land surfaces. It is found that applying over land plays a positive impact for overestimated cloud height along the stratocumulus coastal regions.

42

It is important to note that this issue requires further study. The Cloud Application Team is working with the AMV team and other cloud remote sensing groups to determine an optimal strategy when inversions are present.
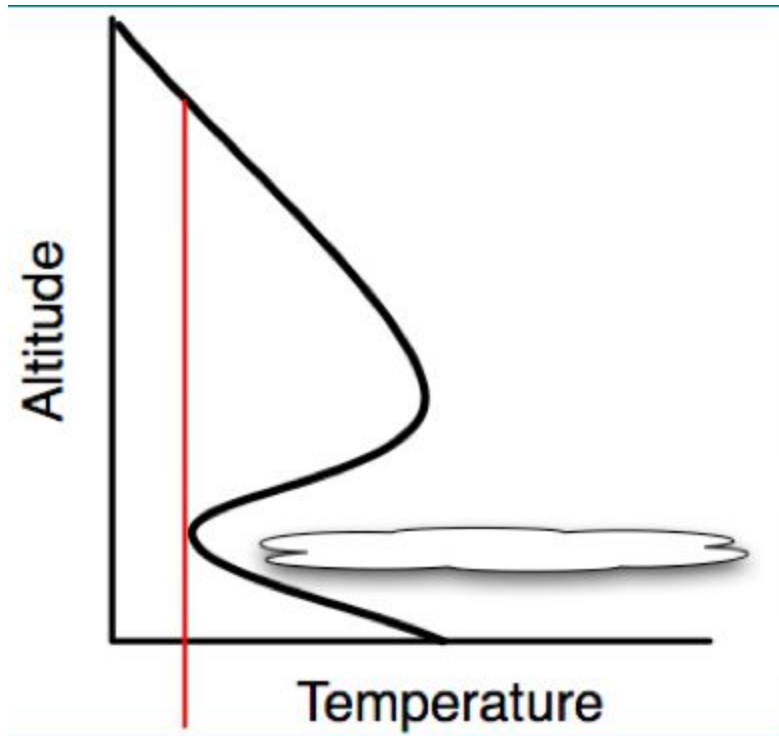
Figure 11 **Illustration of a cloud located in a temperature inversion. (Figure provided by Bob Holz of UW/SSEC).**

4.4.2.9 Computation of Cloud Layer

Another function of the ACHA is to compute the cloud layer for each cloudy pixel. Currently, we classify each pixel into one of three layers (high, middle and low-level). Using the ISCCP definition, we classify clouds with $Pc < 440$ hPa as being in the high layer and clouds with $Pc > 680$ hPa as being low level. Clouds between 440 and 680 hPa are classified as mid level. Subsequent processing is done to take the cloud layer information and generate a cloud cover of each layer.

4.4.2.10 Handling approaches when CO2 absorption channels are unavailable

CO_2 absorption channels near 13 μm are critical for retrieving semi-transparent cirrus cloud heights. However, certain instruments lack these channels and thus the retrieval accuracy of cirrus is reduced. VIIRS onboard Suomi S-NPP and NOAA-20, and the following JPSS-2 missions are examples. In an attempt to compensate for missing CO_2

channels, one approach is to spectrally convolve and spatially interpolate high spectral sounder data near CO_2 absorption channels to the imager resolution. Note that data coverage is limited by the sounder's scanning swath and spatial resolution. Cloud heights can be retrieved from these data, such as from the CO_2 slicing method, which is at a coarser spatial resolution yet provides a valuable additional priori value for cirrus clouds. Another approach is to read in cloud top data provided as part of the sounder products, such as the NOAA Unique Combined Atmospheric Processing System (NUCAPS) products. NUCAPS retrieves two levels of cloud data (cloud fraction and cloud top pressure), and carefully filtered data prove to provide better cloud top products for thin cirrus clouds than retrievals from VIIRS alone.

Revisions are made to the a priori value of cloud temperature and the associated background error variance matrix element to reflect the information from the sounder:

$$x_0(1) = [x_{0s}(1)/S_{as}(1,1) + x_{0i}(1)/S_{ai}(1,1)]/(1/S_{as}(1,1) + 1/S_{ai}(1,1))$$
$$S_a(1,1) = [1/S_{as}(1,1) + 1/S_{ai}(1,1)]^{-1}$$

(Eq. 36)

where x_{0s} and x_{0i} stand for the a-priori values from sounder and imager, respectively, and similarly for S_a. This approach benefits from both the sounder's spectral information and imager's high spatial resolution. Meanwhile, it preserves the integrity of the OE approach without fundamental modifications.

The other approach is called the "FUSION" method. Unlike the previous approach, this generates a 13.3 μm BT based on a statistical reconstruction method (Cross et al. 2013) with no gaps.

4.4.2.11 IR Cloud Optical Properties

ACHA generates IR based optical properties, including cloud optical depth and effective particle size. The IR based retrieval are very sensitive to thin optical depth and small particle size compared to daytime solar reflectance based bispectral method. Plus, it provides consistent day and night retrievals.

As discussed in 3.4.1.3, the microphysical parameter β and particle size can be parameterized by a polynomial relationship. Since β is an ACHA output, particle size can be obtained from pre-computed coefficients. Subsequently, scattering properties in Eq. (5) can be determined from particle size using similar polynomial relationships. The next step is to estimate optical depth. The absorption optical depth τ_{abs} can be estimated from cloud emissivity e_c:

$$\tau_{abs} = -\mu \, ln(1 - e_c) \qquad\qquad \text{(Eq. 37)}$$

44

where μ is the cosine of the viewing zenith angle. The full optical depth at visible wavelength is derived by

$$\tau_{vis} = \frac{\sigma_{vis}}{\sigma_{11\mu m}} \frac{\tau_{abs}}{1 - \omega_{11\mu m} g_{11\mu m}}$$

(Eq. 38)

4.4.2.12 Parallax correction

If the satellite viewing angle is large, clouds are displaced relative to the surface. This shift is called parallax and it increases as cloud height increases. Figure 12 provides an illustrative example showing the parallax displacement from dotted to solid shaded surfaces.

Earth's Surface
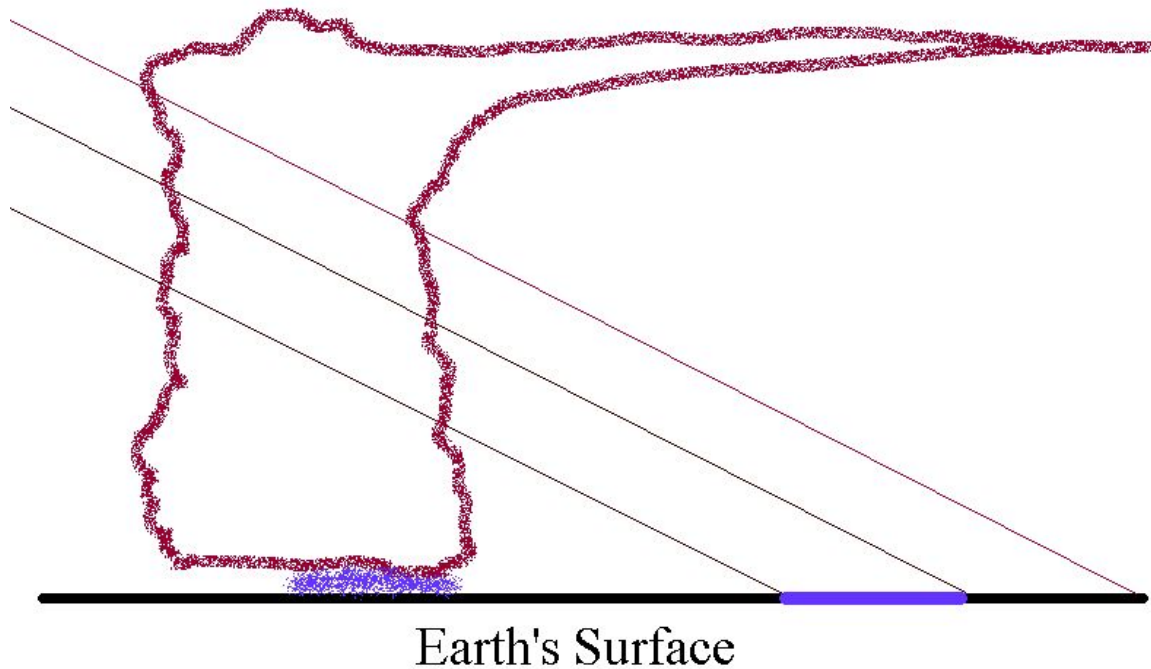
Figure 12 **Illustration of the parallax displacement. (Figure provided by Scott Lindstrom of UW/SSEC).**

Parallax correction is necessary under this situation and the following steps are performed to the latitude and longitude.

$$lon_{per\ meter} = lat_{per\ meter} / cos(latitude)$$ (Eq. 39)
$$\Delta lat = (Z_c - Z_s) * tan(\theta) * cos(\varphi) * lat_{per\ meter}$$ (Eq. 40)
$$\Delta lon = (Z_c - Z_s) * tan(\theta) * sin(\varphi) * lon_{per\ meter}$$ (Eq. 41)

45

where $lat_{per\ meter}$ indicates the change of latitude in degree per meter and a constant of value $8.9932 \times 10^{-6}\ m^{-1}$ is used, $lon_{per\ meter}$ is the change of longitude per meter, Z_c is cloud top height, Z_s is surface height, θ is satellite zenith angle, φ is satellite azimuth angle, and Δlat and Δlon are the shifts due to parallax.

And parallax corrected latitude lat_{pc} and longitude lon_{pc} are

$$lat_{pc} = latitude + \Delta lat \qquad\qquad\qquad \text{(Eq. 42)}$$
$$lon_{pc} = longitude + \Delta lon \qquad\qquad\qquad \text{(Eq. 43)}$$

4.4.3 Algorithm Output

4.4.3.1 Output

The output of the ACHA provides the following ABI cloud products listed in the F&PS:
- Cloud-top temperature,
- Cloud-top pressure,
- Cloud-top height, and
- Cloud cover layer.

All of these products are derived at the pixel level for all cloudy pixels. Example images of the above products are provided in Section 4.2.

4.4.3.2 Intermediate data

The ACHA derives the following intermediate products that are not included in F&PS, but are used in other algorithms, such as the atmospheric motion vector (AMV) algorithm:
- Error estimates,
- Cloud 11 μm emissivity, and
- Cloud microphysical index (β)
- Lower level cloud-top temperature
- IR retrieved cloud optical depth
- IR retrieved cloud particle size
- Optimal estimation cost function
- Parameter Quality Indicator
- Parallax corrected latitude/longitude
- Ice cloud fraction

The Parameter Quality Indicator is a discretized and normalized version of the error estimates. It is not a substitute for the product quality flag (see below). A detailed description of the parameter quality indicator is provided in section 3.4.2.4.

4.4.3.3 Product Quality Flag

In addition to the algorithm output, a pixel level product quality flag will be assigned. The possible values are as follows:

Flag Value	Description
0	Fully successful retrieval
1	Marginally successful retrieval
2	Retrieval attempted and failed
3	No retrieval attempted

4.4.3.4 Processing Information Flag

In addition to the algorithm output and quality flags, processing information, or how the algorithm was processed, will be output for each pixel. If the bit is 0, then the answer is no, and if the bit is 1, the answer is yes.

Bit	Description
1	Cloud Height Attempted
2	Bias Correction Employed
3	Ice cloud retrieval
4	Local Radiative Center Processing Used
5	Multi-layer Retrieval
6	Lower Cloud Interpolation used
7	Boundary Layer Inversion Assumed
8	NWP Profile Inversion Assumed

4.4.3.5 Metadata

In addition to the algorithm output, the following will be output to the file as metadata for each file:
- Mean, Min, Max and standard deviation of cloud top temperature;
- Mean, Min, Max and standard deviation of cloud top pressure;
- Mean, Min, Max and standard deviation of cloud top height;
- Number of QA flag values ;
- For each QA flag value, the following information is required:
  - Number of retrievals with the QA flag value,
  - Definition of QA flag,
  - Total number of detected cloud pixels, and
  - Terminator mark or determination.

5 Test Datasets and Outputs

5.1 Proxy Input Datasets

S-NPP VIIRS data are available at the time of writing this ATBD. However, MODIS data is used instead as proxy data for two reasons. First, MODIS is recognized as a successful project, so validating again MODIS MYD06 product is critical to test ACHA performance across sensors. MODIS has the needed channel information (8.5, 11 and 12 μm) for ACHA to run on VIIRS mode. By using MODIS as proxy data, the convenience of direct comparisons among MYD06, ACHA MODIS and ACHA VIIRS are possible without making collocation. Second, by using 5-km reduced resolution MODIS data, compared to 750m moderate resolution S-NPP VIIRS data, the retrievals and comparisons can be done in a relatively fast way without compromising data integrity. As described below, the data used to test the ACHA are from Aqua MODIS observations on January 1, 2013 collocated with CALIPSO data. ACHA is run on mode 10 for ABI, which is the default mode for MODIS. Additionally, run on mode 9 is conducted to mimic the VIIRS sensor as discussed in Table 3.

The rest of this section describes the proxy and validation datasets used in assessing the performance of the ACHA.

5.1.1 MODIS Data

MODIS provides 36 spectral channels with a spatial resolution of 250 m (band 1-2), 500 m (band 3-7) and 1000 m (band 8-36). MODIS provides an adequate source of proxy data for testing and developing the ACHA. One day of Aqua 5-km resolution MODIS level 2 data from January 1, 2013 were generated from two ACHA modes and collocated with CALIPSO is saved, and global subset level2b data in 0.1 degree resolution are also generated. The Aqua MODIS data were provided by the UW/SSEC Data Center and processed for the datasets specified in section 4.1.

5.1.2 CALIPSO Data

With the launch of CALIPSO and CloudSat into the NASA EOS A-Train in April 2006, the ability to conduct global satellite cloud product validation increased significantly. Currently, CALIPSO cloud layer results are being used to validate the cloud height product of the ACHA. The CALIPSO data used here are the 1 km cloud layer results. There are also 5 km data available and merged 1 km and 5 km were used to make use of the high resolution of the 1 km data and enhanced cirrus detection of the 5 km data (Heidinger et al., 2019). Figure 13 shows an example of CALIPSO profiles used in this study.

48
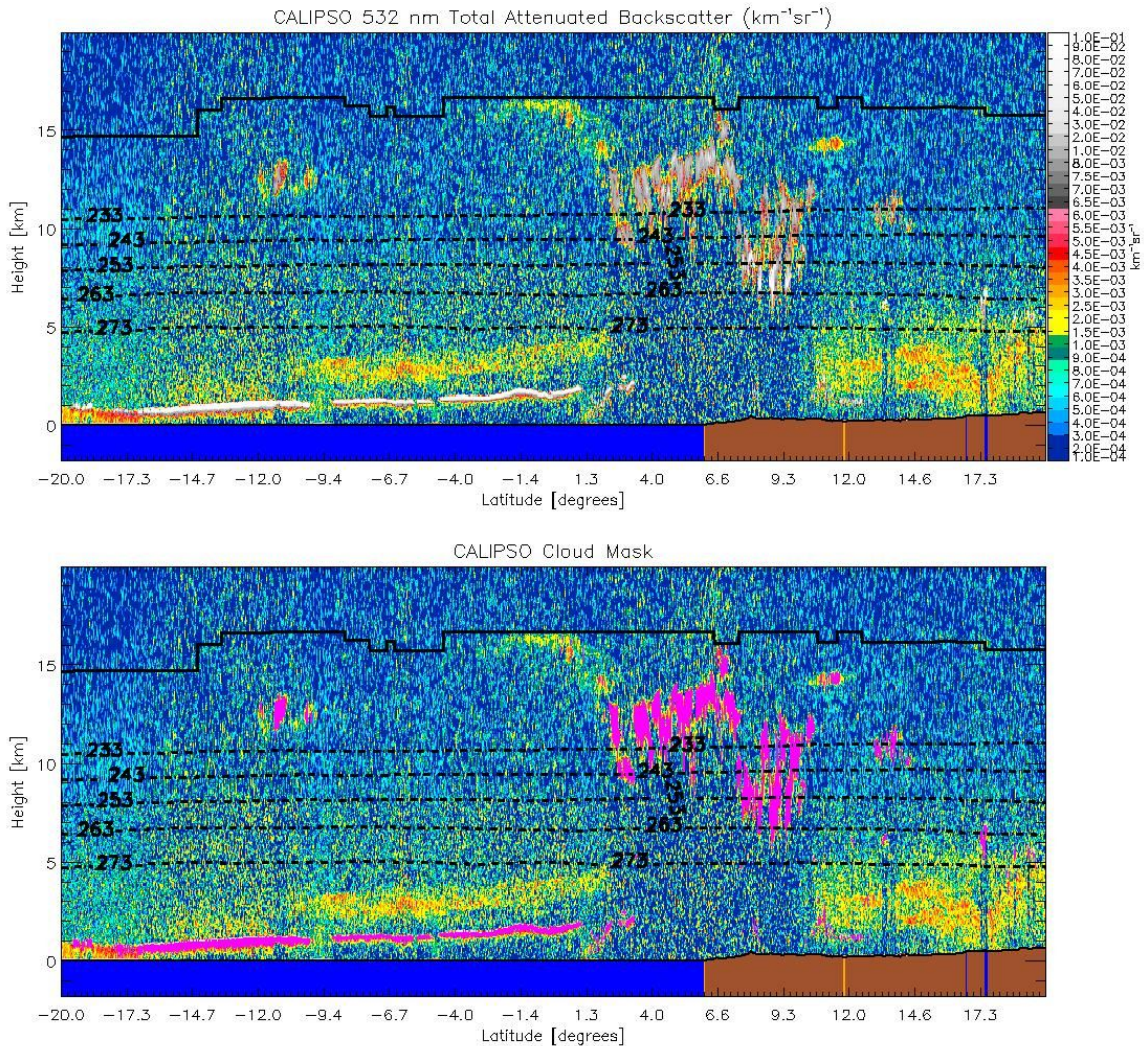
Figure 13 **Illustration of CALIPSO data used in this study. Top image shows a 2D backscatter profile. Bottom image shows the detected cloud layers overlaid onto the backscatter image. Cloud layers are colored magenta. (Image courtesy of Michael Pavolonis, NOAA)**

5.2 Output from Simulated/Proxy Inputs Datasets

The ACHA result was generated using the MODIS data from the dataset specified in section 4.1. During both the TRR and subsequent tests, comparisons between the online and offline (Cloud AWG) output of the ACHA, when the same inputs were used, showed an exact match of the height, temperature and pressure outputs. These tests were conducted under different conditions using the same input for both the online and offline tests. Figures 14-18 shown below illustrate the ACHA cloud-top temperature, pressure, height, cloud layer and cloud emissivity. These images correspond to global ascending tracks on January 1, 2013 and top and bottom images correspond to VIIRS and MODIS ACHA modes respectively.

Figure 14 **Example ACHA output of cloud-top temperature derived from MODIS proxy data for VIIRS (top) and MODIS (bottom) on January 1, 2013.**

50

Figure 15 **Example ACHA output of cloud-top pressure derived from MODIS proxy data for VIIRS (top) and MODIS (bottom) on January 1, 2013.**

Figure 16 **Example ACHA output of cloud-top height derived from MODIS proxy data for VIIRS (top) and MODIS (bottom) on January 1, 2013.**
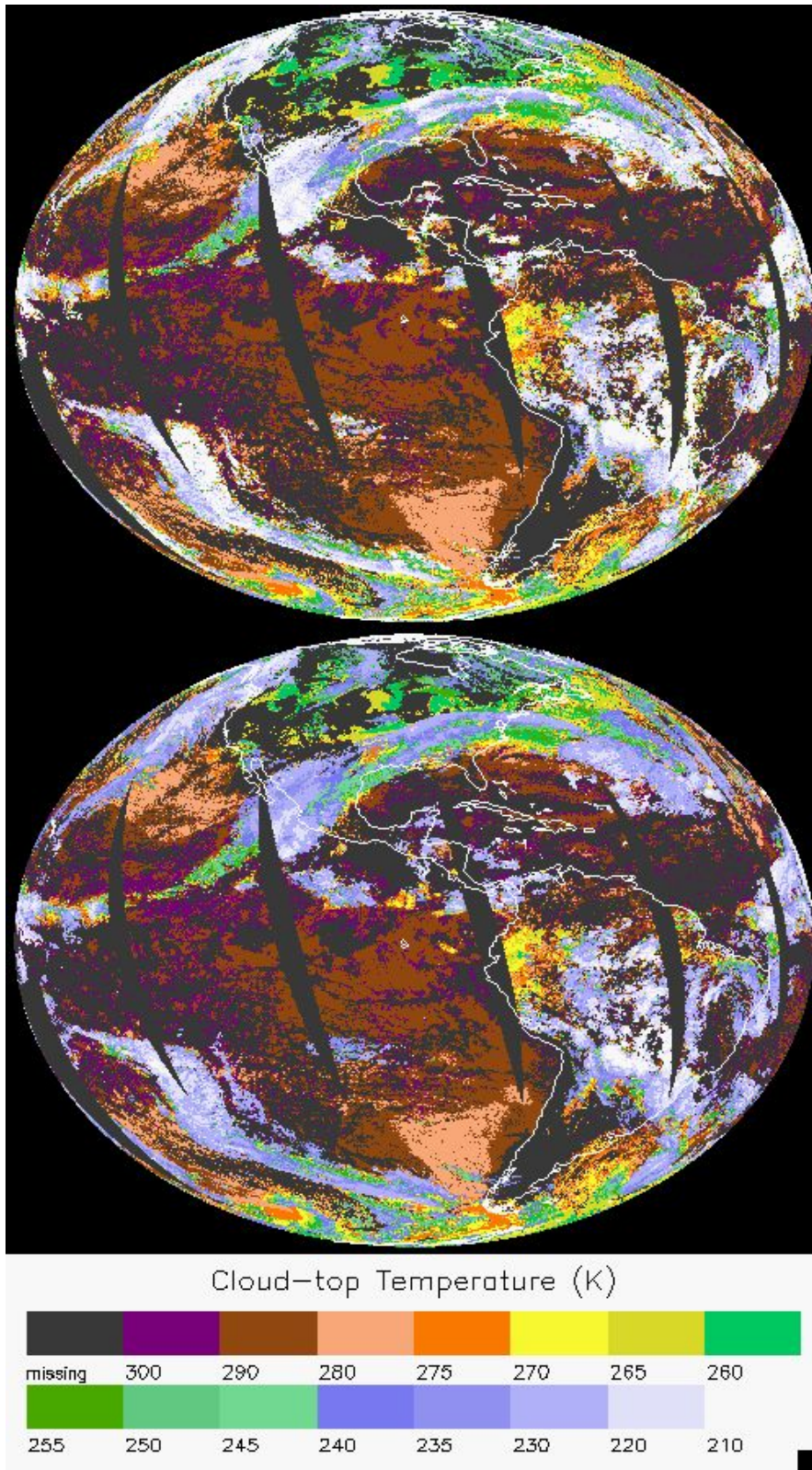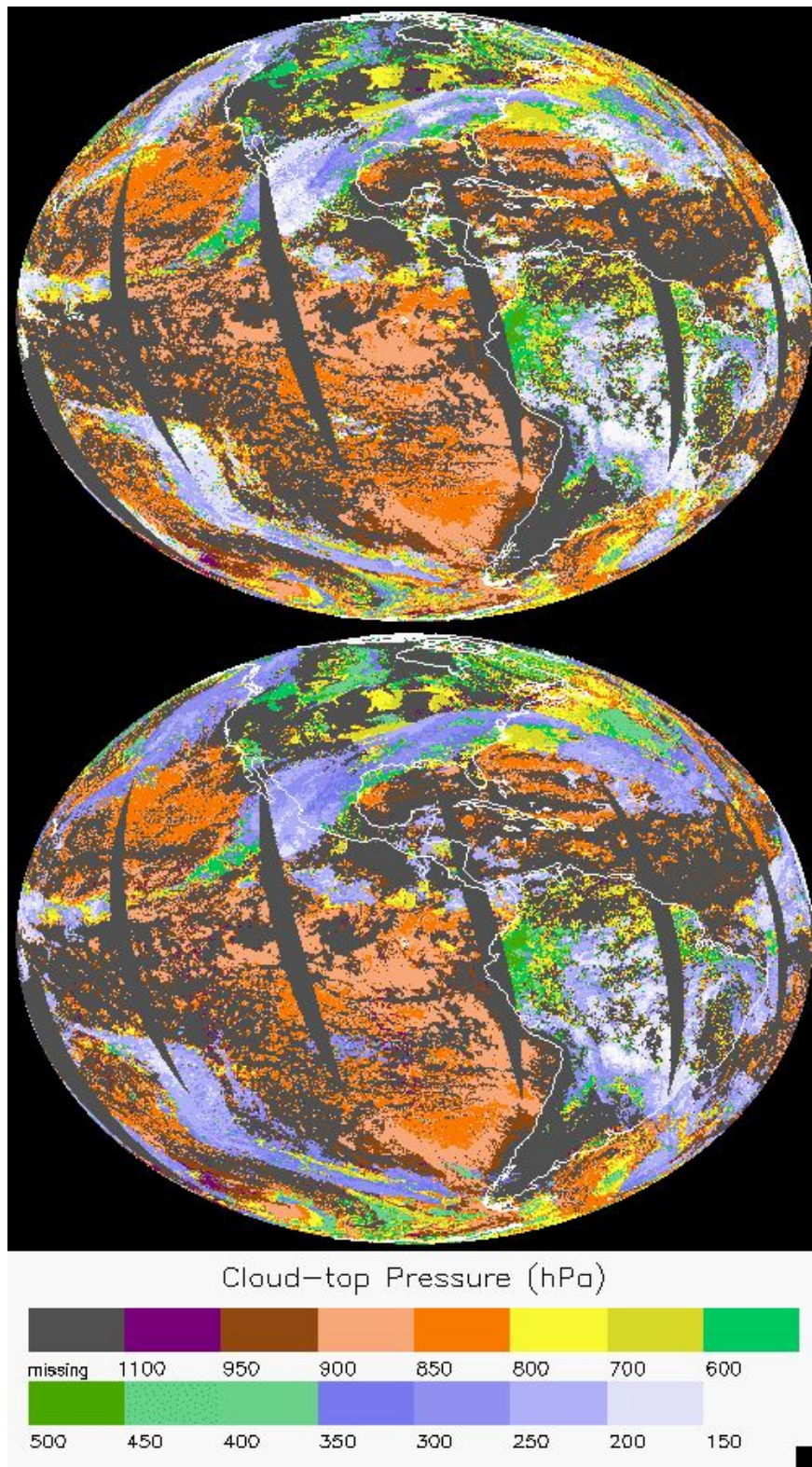
Figure 17 **Example ACHA output of cloud layer derived from MODIS proxy data for VIIRS (top) and MODIS (bottom) on January 1, 2013.**
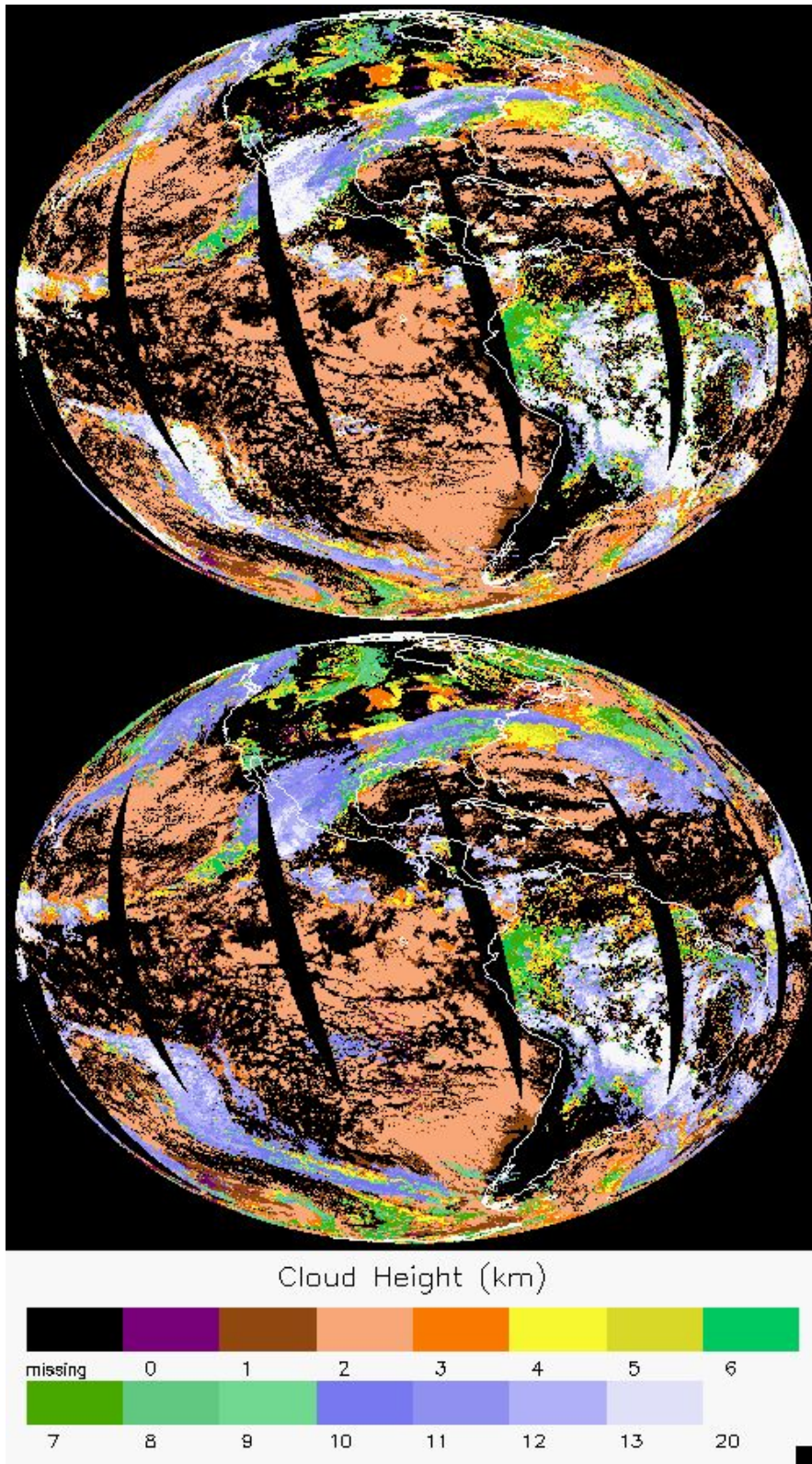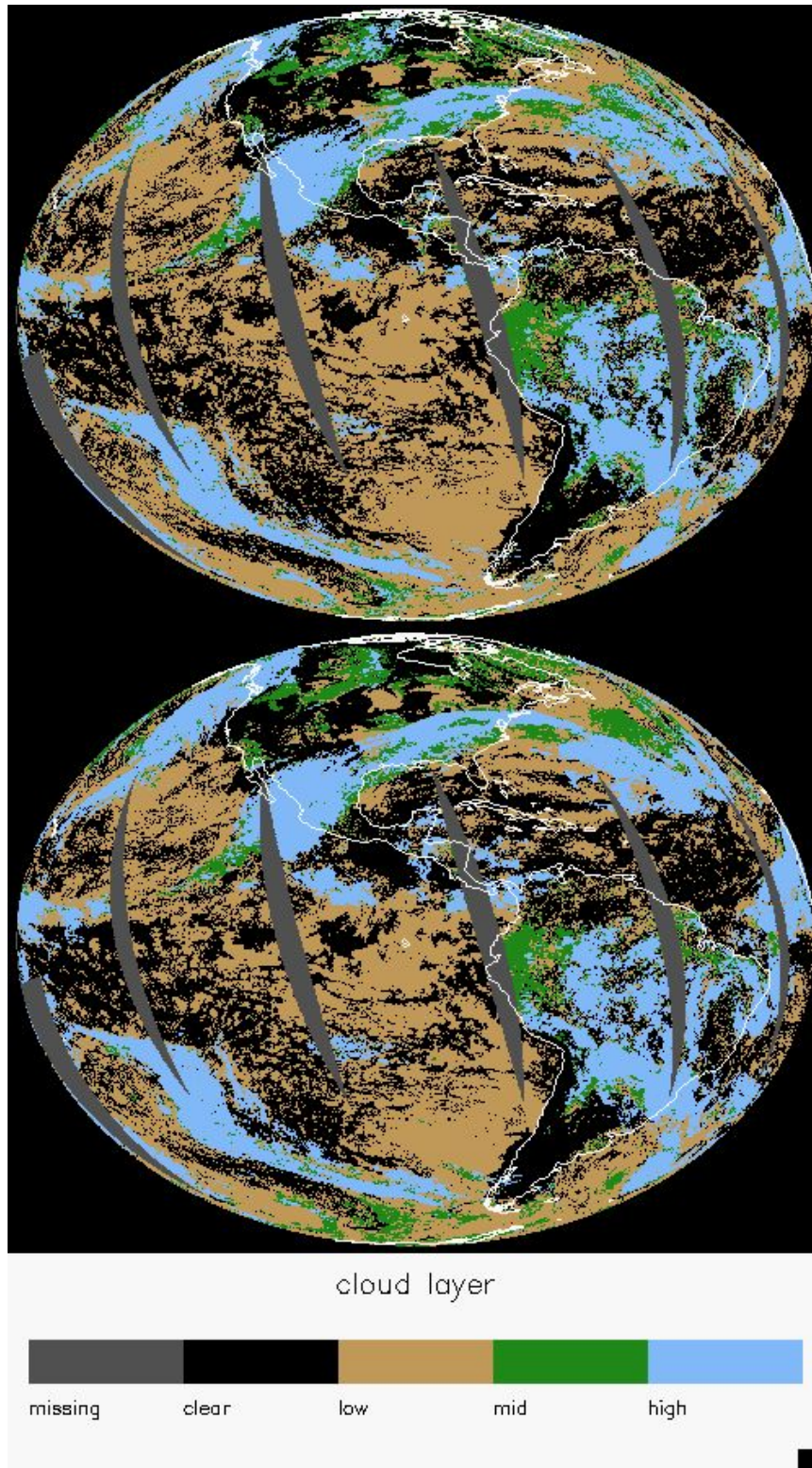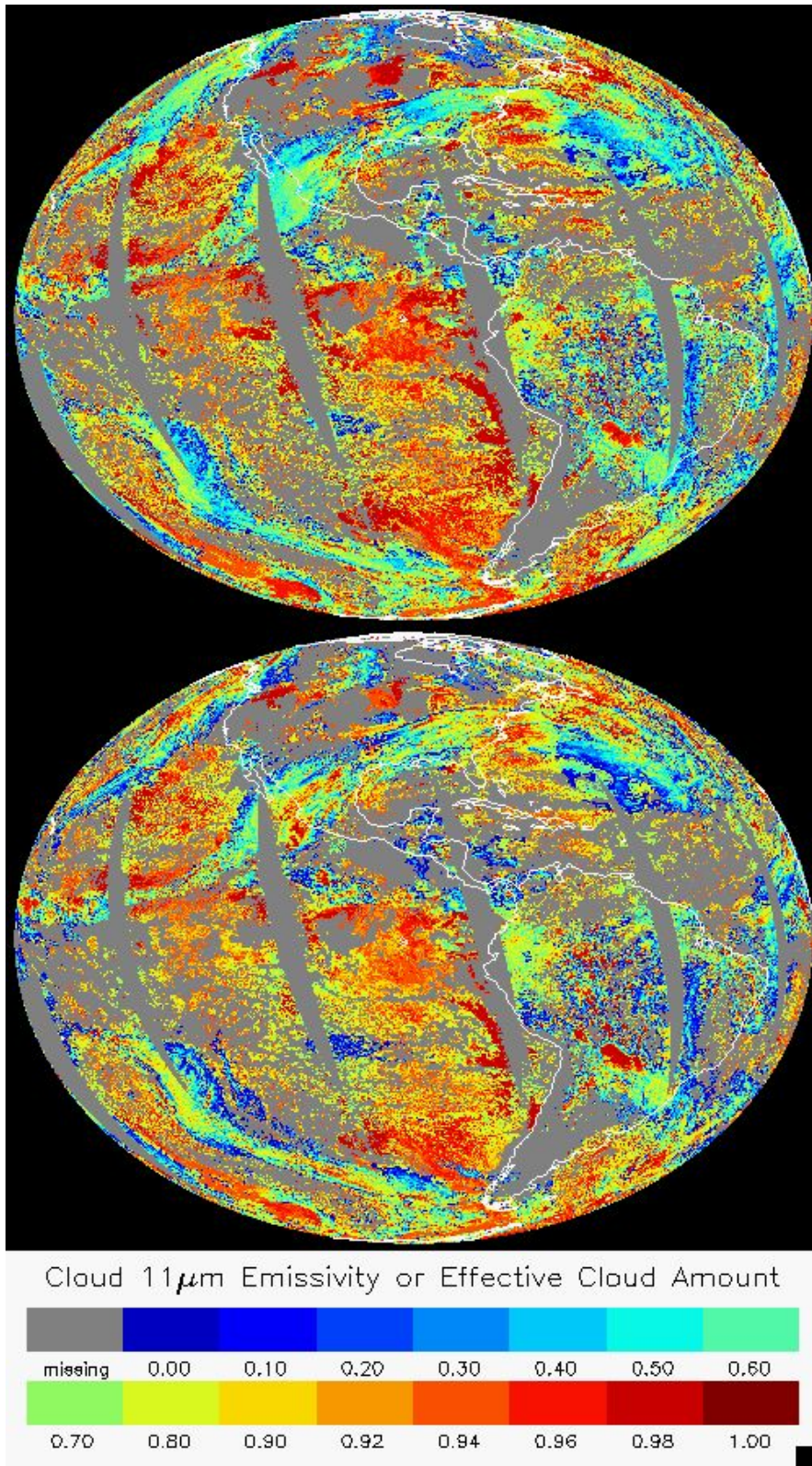
Figure 18 **Example ACHA output of 11 μm cloud emissivity derived from MODIS proxy data for VIIRS (top) and MODIS (bottom) on January 1, 2013.**

5.2.1 Precisions and Accuracy Estimates

To estimate the precision and accuracy of the ACHA, CALIPSO data from NASA EOS A-Train are used. This new data source provides unprecedented information on a global scale. While surface based sites provide similar information, the limited sampling they offer requires years of analysis to generate the amount of collocated data provided by CALIPSO in a short time period. Various MODIS data has also proven to be useful in assessing the quality of ACHA.

5.2.1.1 MODIS Analysis

The MODIS cloud height products (MYD06) have proven to be a useful and accurate source of information to the cloud remote sensing community. The MYD06 cloud height algorithm employs the longwave CO_2 channels in a CO_2 slicing approach to estimate the cloud-top pressure and cloud effective cloud amount. More details on this algorithm are available in the MODIS MYD06 ATBD (Menzel et al., 2006). The MODIS MYD06 ATBD quotes the cloud-top pressure accuracy to be roughly 50 mb, which is under the GOES-R ABI specification of 100 mb.

Given the wide use of the MYD06 product set, a comparison between the ACHA and MYD06 is warranted. While the MYD06 product set does provide the direct measure of cloud height provided by CALIPSO, it does complement the verification by providing qualitative comparisons over a larger domain. Given the availability of the longwave CO_2 channels on MODIS, we expect MYD06 to provide superior results especially for semitransparent cirrus.

It is also assumed that cloud products should only agree when the cloud detection and phase results agree. An example of this comparison is shown in Figure 19. In this figure, the global ascending track cloud-top height data in 0.1 degree resolution for January 1, 2013 as shown above are compared on a phase-matched basis. The left panel shows the comparison for ACHA VIIRS against MYD06 and right for ACHA MODIS.

The results indicate that the height differences between ACHA and MYD06 are less than 1km and the correlations are above 0.9. Although comparing two passive satellite measurements cannot be thought of as validation, the bias and precision estimates of the ACHA relative to MODIS indicate the AWG algorithm is performing well. The cloud-top height comparison also shows that the ACHA algorithm is meeting specification relative to MODIS for this scene.
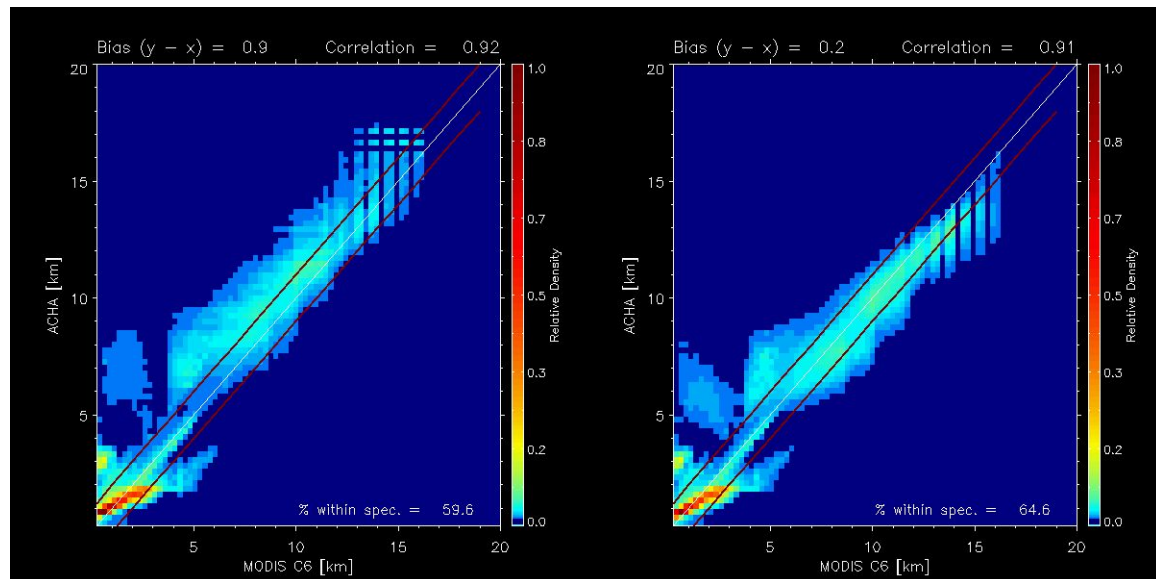
Figure 19 **Comparison of phase-matched cloud-top height for ACHA derived from MODIS proxy data against MYD06 Collection 6 (C6) products. Left shows VIIRS (mode 9) and right shows MODIS (mode 10).**

5.2.1.2 CALIPSO Analysis

The CALIPSO/CALIOP lidar data (hereafter referred to as CALIPSO) provide unique information on the cloud vertical structure that can be used to validate the ACHA. For this analysis, a collocation tool has been developed to determine the relevant information provided by CALIPSO for each collocated MODIS pixel. This tool has been applied to all MODIS data for the datasets specified in section 4.1. This tool also works with any satellite that ACHA supports. For each MODIS pixel that is collocated with CALIPSO data, the following information is available:

- Time difference between MODIS and CALIPSO,
- Number of cloud layers observed by CALIPSO,
- Cloud-top height of highest cloud layer, and
- Cloud-top temperature of highest cloud layer

In addition to the above information, the MODIS 11 μm radiances and the computed clear-sky radiances are used to estimate the cloud emissivity assuming the cloud existed at the height given by CALIPSO. The analysis shown in this section proves the good performance of the ACHA based on the cloud height and cloud emissivity as derived from CALIPSO. The height bins were set to a width of 2 km thick and range from 0 to 16 km. The cloud emissivity bins were set to a width of 0.2 and range from -0.2 and 1.2. Emissivities less than 0 imply the observed radiance was less than the clear-sky radiance and emissivities greater than 1.0 imply that the observed radiance was greater than the

56

blackbody emission at the CALIPSO cloud temperature. Only data that were called cloudy by the GOES-R AWG cloud mask (ACM) and by CALIPSO were included in this analysis. Figure 20 shows the relative distribution of pixels in Z_c-e_c space for this analysis. Any cells that are colored dark did not have enough points for analysis.
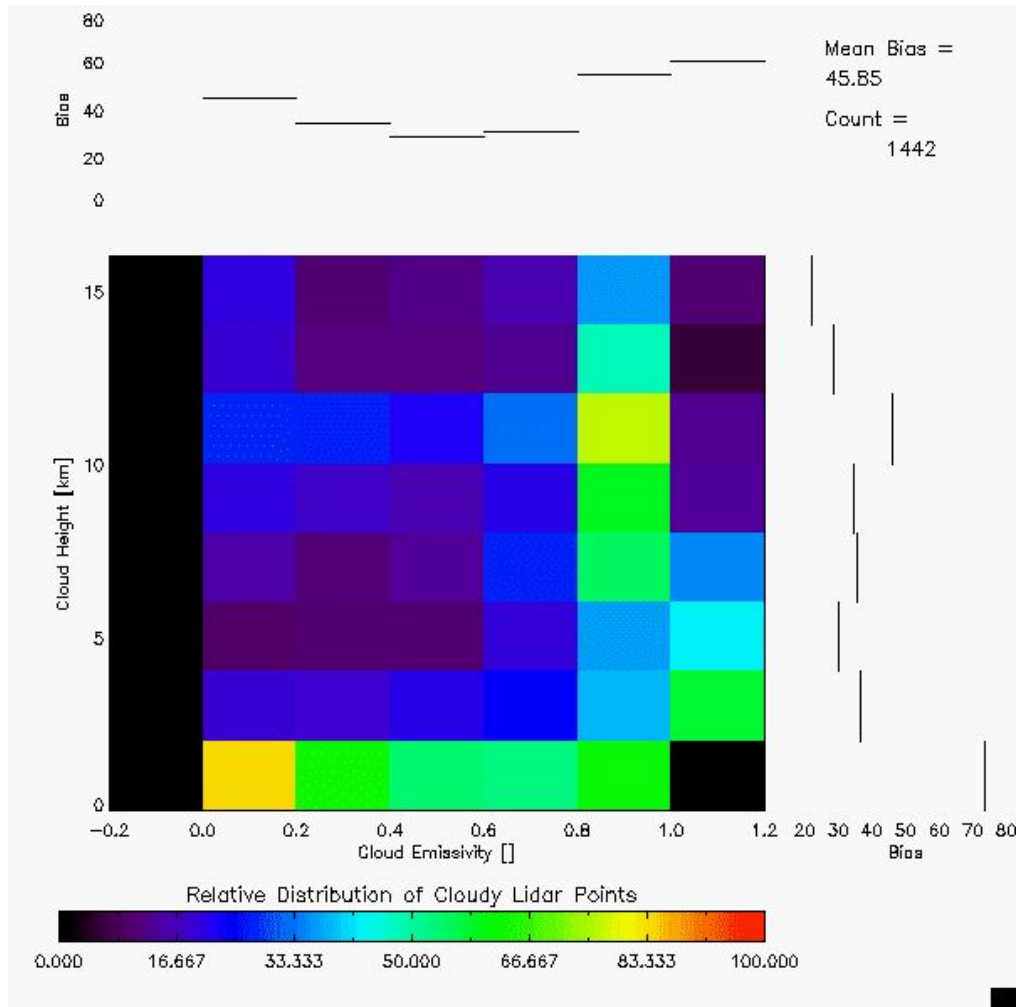
Figure 20 **Relative distribution of points used in the validation of the ACHA applied to MODIS data for data observed during simultaneous MODIS and CALIPSO periods on January 1, 2013.**

5.2.1.2.1 Validation of Cloud Top Height

For each Z_c – e_c bin, the mean bias in the ACHA – CALIPSO results was compiled. The mean bias is the accuracy. The resulting distributions of the mean of the bias is shown in Figure 21 for both VIIRS and MODIS. The VIIRS specification for accuracy is 1 km for clouds with $e_c > 0.6$ and 2 km when $e_c < 0.6$. While the accuracy is below this value for nearly all stated cloudiness stratifications, there is exception for VIIRS high clouds, in particular optically thin cirrus. This is primarily due to missing LW CO_2 absorption channels. Work is being done to improve in this area as well and involves incorporating

radiance biases to improve our ability to reproduce the cirrus observations and use of the hyperspectral sounder CO_2 channels discussed in 3.4.2.10 to increase the sensitivity to cloud height for these clouds.

Figure 21 **Distribution of cloud-top height mean bias (accuracy) as a function of cloud height and cloud emissivity as derived from CALIPSO data for MODIS observations. Bias is defined as ACHA – CALIPSO. Left shows for VIIRS and right for MODIS.**

5.2.1.2.2 Validation of Cloud Top Temperature

The same analysis was applied to the verification of cloud-top temperature. The resulting accuracy of the bias results are shown in Figure 22. As expected, the T_c results show the same pattern as the Z_c results. The VIIRS specification for accuracy for cloud-top temperature is 3 K and 6 K for clouds with e_c greater and less than 0.6, respectively. About half of the observed clouds meet these restrictions.
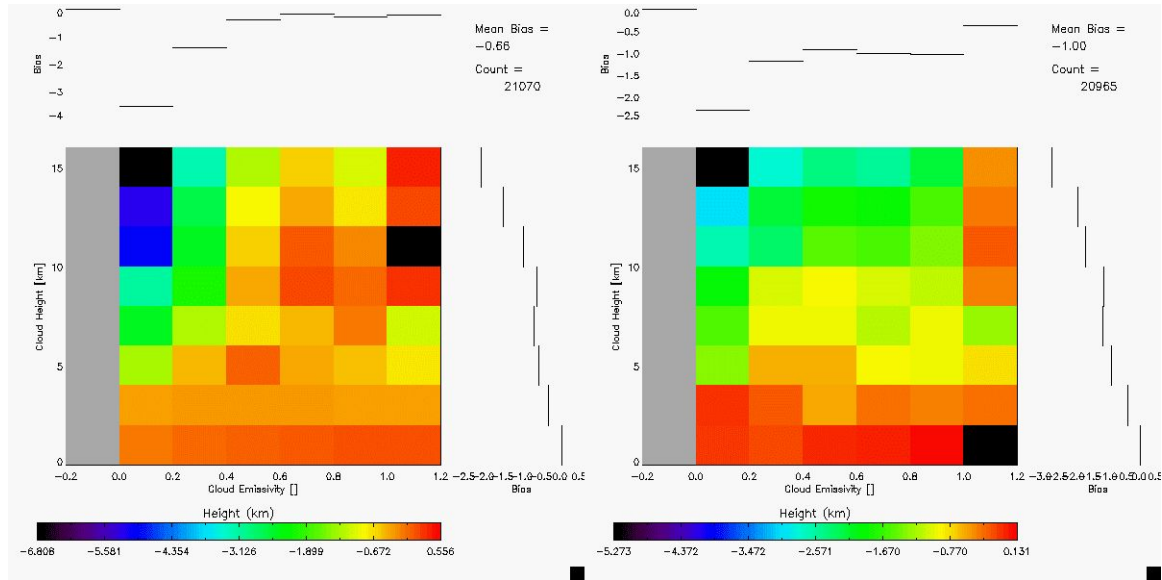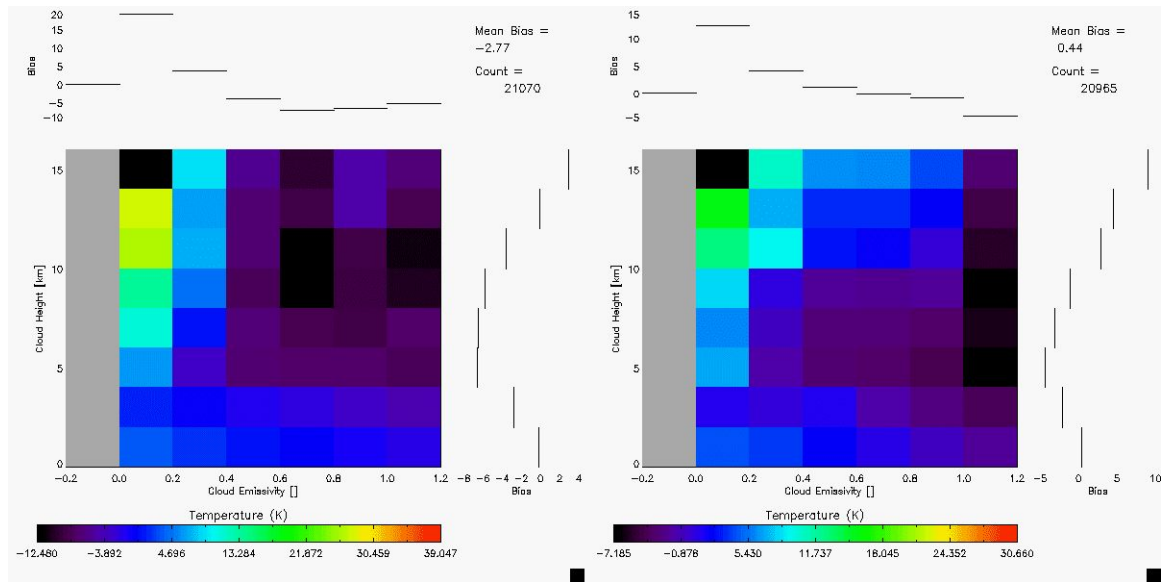
Figure 22 **Distribution of cloud-top temperature mean bias (accuracy) as a function of cloud height and cloud emissivity as derived from CALIPSO data for MODIS observations. Bias is defined as ACHA – CALIPSO. Left shows for VIIRS and right for MODIS.**

5.2.1.2.3 Validation of Cloud Top Pressure

The current suite of CALIPSO products does not include pressure as a product. We are modifying our tools to estimate cloud pressure from the cloud height products in the CALIPSO product suite. However, the cloud-top pressure errors are highly correlated to the cloud-top height errors shown above. The comparisons to MODIS confirm this correlation.

5.2.1.2.4 Validation of Cloud Layer

The cloud layer product has been defined as a flag that indicates where a cloud-top falls within 3 discrete vertical layers in the atmosphere. These layers are defined as follows:

- Low: pressures between the surface and 680 hPa,
- Mid: pressures between 680 and 44 hPa, and
- High: pressures lower than 440 hPa.

These layers are the standard layers used in many cloud product systems such as those used in the International Satellite Cloud Climatology Project (ISCCP). Cloud amounts in these layers have often been used for verifying cloud parameterization in NWP forecasts.

As mentioned above, CALIPSO does not generate a standard cloud-top pressure product so direct validation of the cloud layer product using CALIPSO is not possible. However, CALIPSO does generate a product whereby the low layer is defined as clouds with top

heights less than 3.25 km, the mid layer is defined as clouds with tops between 3.25 and 6.5 km and the high layer is defined as clouds with tops higher than 6.5 km. These height layers roughly correspond to the pressure layers used to define the VIIRS product.

At preparation of this ATBD for VIIRS, there is no direct comparison of VIIRS layers and CALIPSO. However, we previously conducted a comparison based on simulated ABI cloud products. Using the CALIPSO layer height definitions, a height-based layer can be derived from the ABI cloud-top heights. In addition, the CALIPSO cloud-top heights of the highest layer can be computed into height-based layer flags. When the CALIPSO and ABI height-based cloud layer flags are compared, a POD value of 91.4 % is computed. The data used in this comparison are the 10-week of SEVIRI runs to simulate ABI. This level of agreement indicates the ABI cloud layer product meets its accuracy specification of 80%. At this time, there is no precision specification placed on this product.

5.2.1.2.5 Validation of IR Cloud Optical Properties

IR retrieved cloud optical properties have also been validated against different data sources, as shown in Figure 23 and Figure 24 below. An additional validation source from CALIPSO/IIR is included. Note that the IR cloud product shown here is not from direct ACHA output. Instead, it is computed from the MYD06 emissivity product and produces physically and quantitatively similar variables from ACHA. The figures are adapted from Heidinger et al. (2015). The results indicate that both cloud optical depth and effective particle size are consistent with existing validation datasets. Therefore, these ACHA products can serve as a reliable dataset for thin cirrus studies for both day and night conditions.
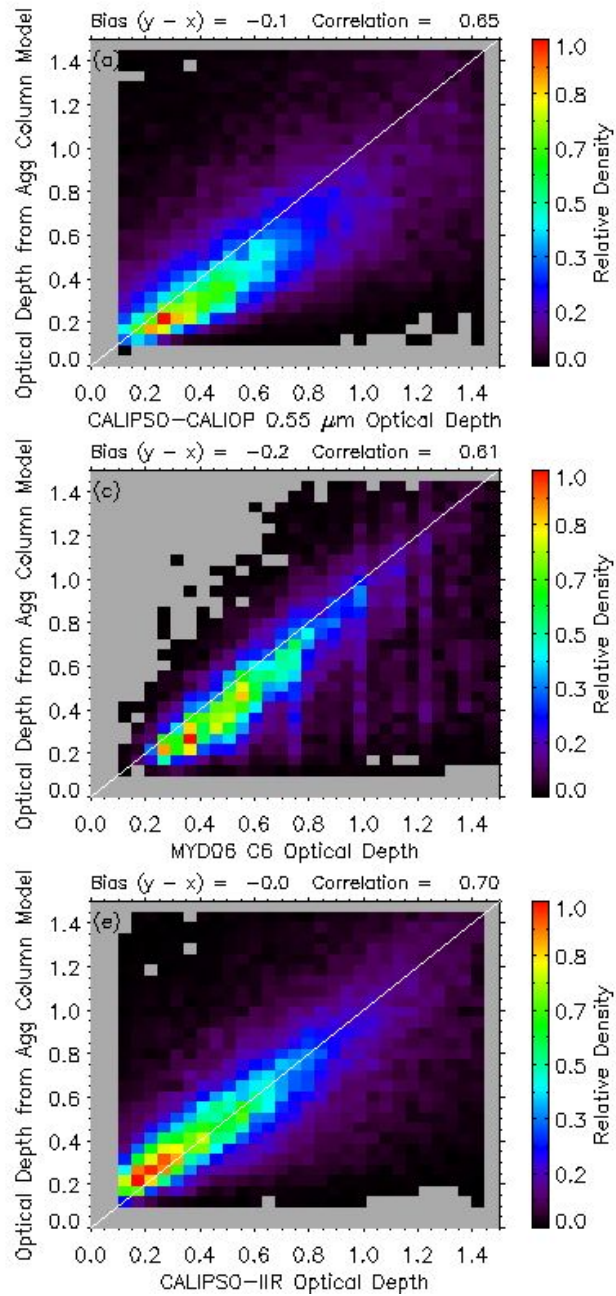
Figure 23 **Comparison of the IR cloud optical depth retrievals. Top panel compares to the CALIPSO/CALIOP, middle panel compares to the C6 MYD06 retrievals, and bottom panel compares to CALIPSO/IIR**.
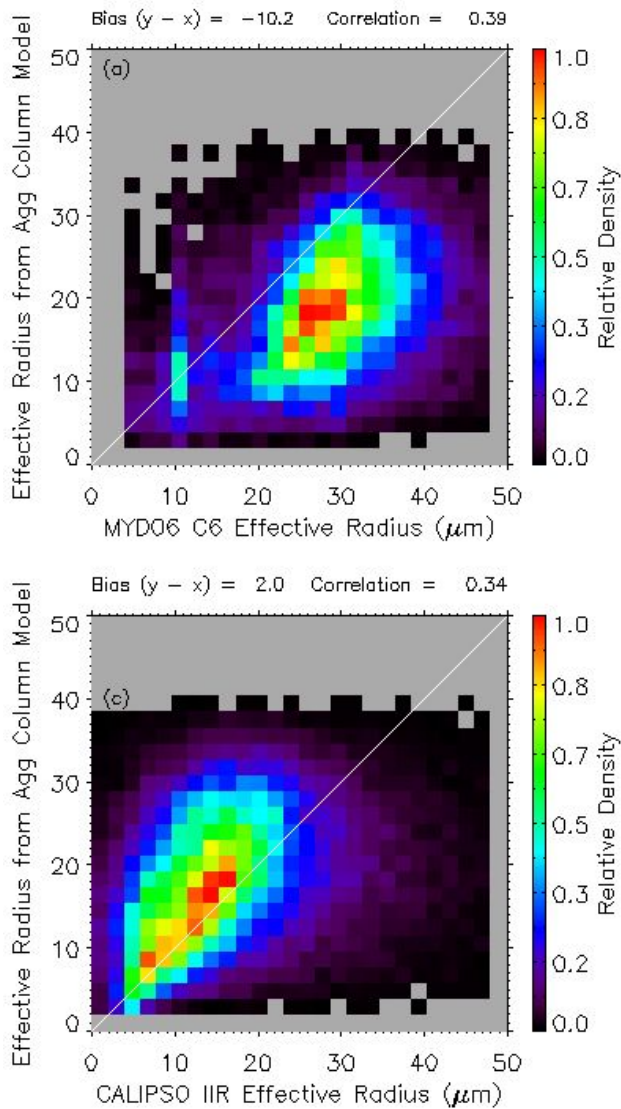
Figure 24 **Comparison of the cloud effective radius retrievals. Top panel compares to the C6 MYD06 retrieval, and the bottom panel compares to CALIPSO/IIR.**

5.2.1.3 Polar Warping

Polar warping is a method to use MODIS and VIIRS data as a comparison tool with geostationary satellites (GOES-16/17). The MODIS/Aqua Aerosol, Cloud and Water Vapor Subset (MYDATML2) Collection 6.1 are used. These are 5 minute, 5km level2 swath files. For VIIRS comparisons, 750 meter level2 files are generated from the NOAA development framework, CLAVRx. MODIS or VIIRS granules are collocated with either

the GOES-16 or GOES-17 ABI sensor. The time difference is allowed to be up to 6 minutes between pixel level observations. Each MODIS/VIIRS pixel uses the geostationary satellite's fixed grid navigation routine to see if a pixel is within the ABI domain. Once a match has been located, common cloud products may be compared. There will not be perfect agreement at the pixel scale so the results from these inter-comparisons are more qualitative. These include cloud fraction, cloud temperature, cloud height, cloud pressure, cloud optical depth, cloud phase, and cloud effective radius. The polar warping comparisons have proven useful in GOES-16/17 Provisional Peer Stakeholder–Product Validation Reviews (PS–PVRs) from May, 2019. Similar comparisons will be used for Full Validation reviews as well Figure 25 shows a MODIS granule warped with GOES-17 from December 2, 2018 at 2020 UTC. The cloud phase from MODIS and GOES-17 is observed in the left column. This is a simple phase representation with blue colors indicating water clouds and white showing ice clouds. The middle column shows the cloud EDR for both MODIS and GOES-17. In this case the product is cloud top pressure. In the right column the GOES-17 false color image is shown on the top. The bottom is a scatter plot for this time period with mostly upper level clouds observed. On a typical day there might be roughly 40 MODIS granules that transect the GOES-17 ABI domain.
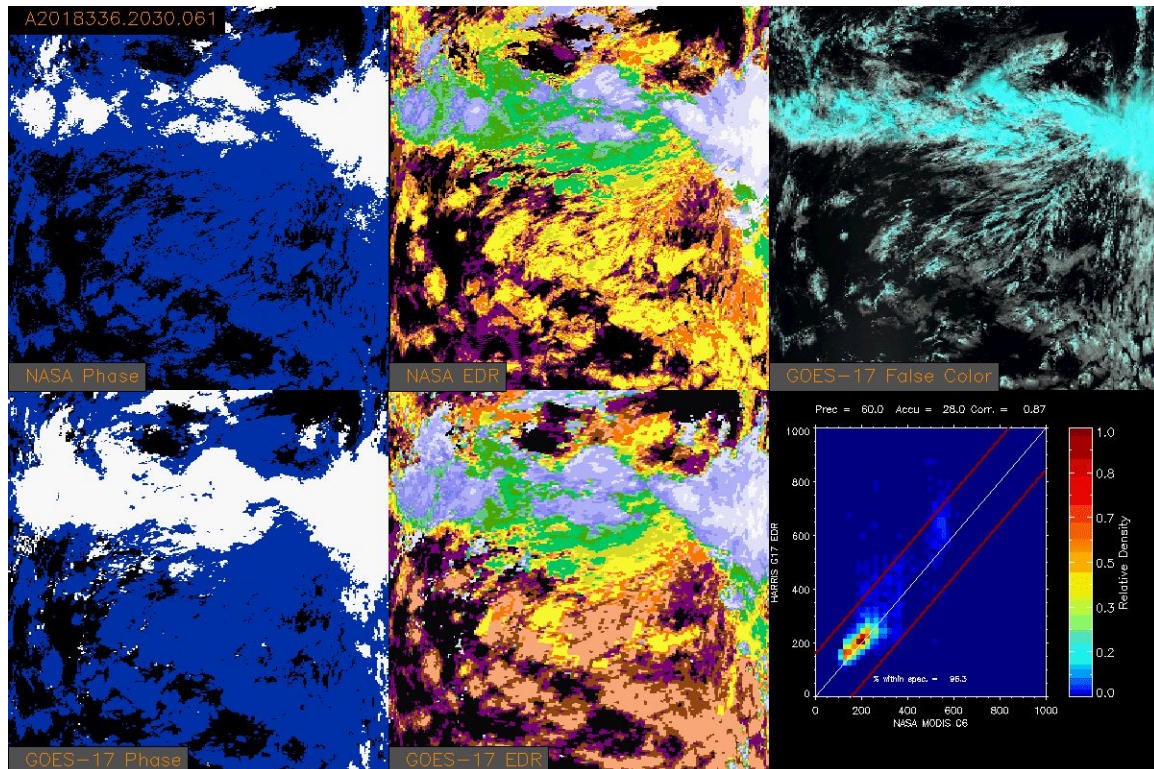

Figure 25 **Polar warping example between MODIS and GOES-17 on December 2, 2018 at 2020 UTC. The phase in the left column is binary with white = ice and water = blue. The middle column shows cloud top pressure for each satellite. The upper right image is a false color GOES-17 image of the warping domain. The lower right image is a scatter plot between the two sensors.**

63
The warping results shown in Figure 25 were used for the GOES-17 Provisional Validation (no LHP events included). Comparisons were made between MODIS and GOES-17 for the month of December 2018. Figure 26 shows the scatter plot for this entire month.
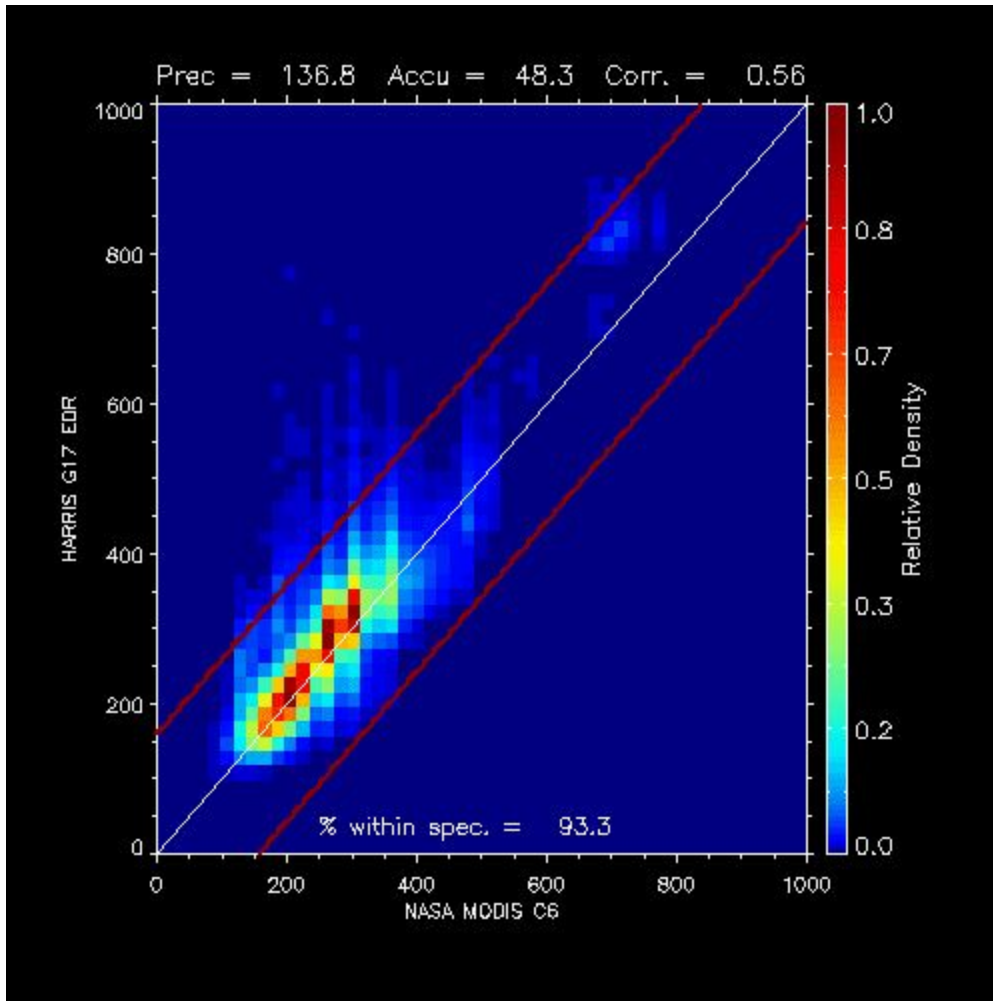
Figure 26 **Scatter plot of cloud top pressure between GOES-17 and MODIS for the month of December 2018.**

The precision and accuracy shown in Figure 26 indicate the GOES-17 products are within specification if MODIS is treated as truth.

Figure 27 is similar to Figure 25. In this case a NOAA-20 VIIRS granule was warped into GOES-16. Future plans for MODIS/VIIRS warping is to get these two processes running in an offline but automated mode. They will become a staple in any upcoming reviews.
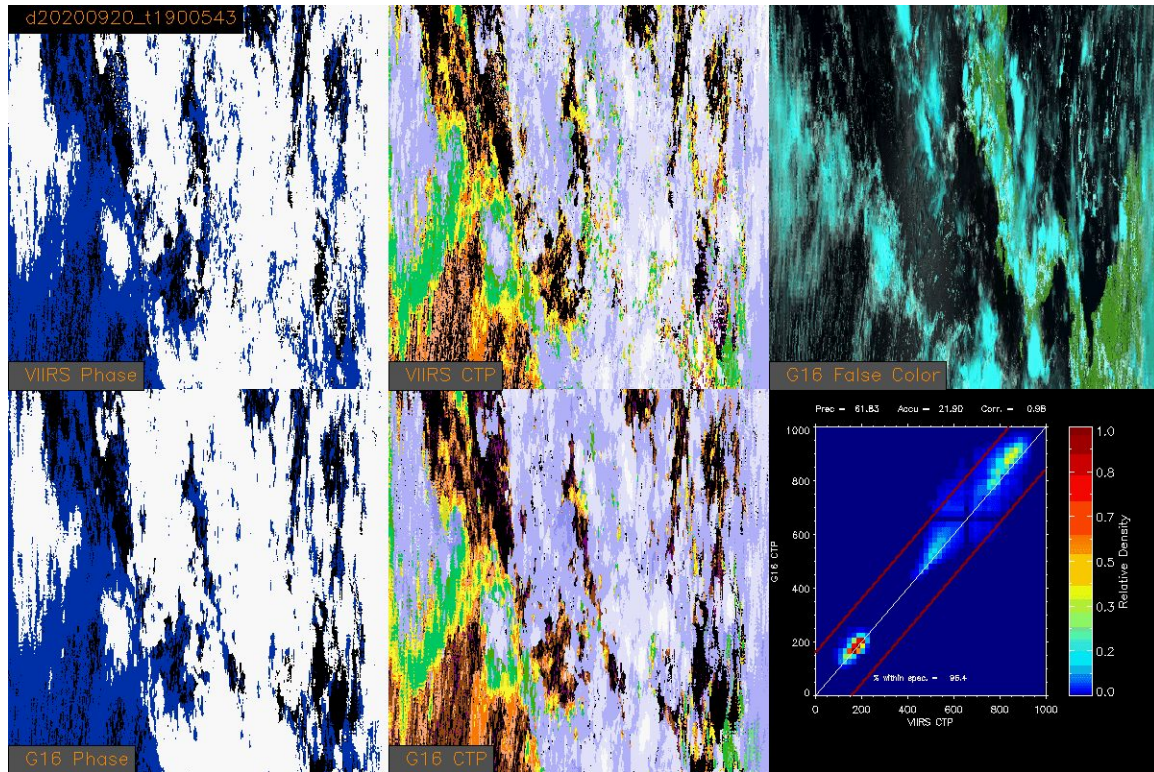
Figure 27 **Polar warping example between NOAA20 VIIRS and GOES-16 on September 20, 2020 at 1900 UTC. The phase in the left column is binary with white = ice and water = blue. The middle column shows cloud top pressure for each satellite. The upper right image is a false color GOES-16 image of the warping domain. The lower right image is a scatter plot between the two sensors.**

5.2.2 Error Budget

Using the validation described above, the following table provides our preliminary estimate of an error budget. The "Bias Estimate" column values most closely match our interpretation of the F&PS accuracy specifications. To match the F&PS, these numbers were generated for low-level clouds with emissivities greater than 0.8. Cloud pressure errors were estimated assuming 1000m = 100 hPa which is a good approximation at low levels.

Table 6 *Preliminary estimate of error budget for ACHA.*

Product	Accuracy and Precision Specification (VIIRS)	Bias Estimate	Standard Deviation Estimate
Cloud-top Temperature	3K when $\tau \geq 1$, 6K when $\tau < 1$	**0.95 K**	**3.65 K**
Cloud-top Height	1km when $\tau \geq 1$, 2km when $\tau < 1$	**0.41 km**	**0.75 km**

Cloud-top Pressure	$\tau \geq 1$: 100mb for [0,3km], 75mb for [3,7km], 50mb for > 7km	-22.6 hPa	47.0 hPa

As Table 6 shows, the ACHA meets the 100% VIIRS requirements for precision and accuracy. It is important to identify the three main drivers of the ACHA error budget.

1. *Lack of Knowledge of Low-level Inversions*. The current F&PS specifications demand accurate performance of cloud height for low-level clouds. Even if the instrument and retrievals are perfect and an accurate cloud-top temperature is estimated, the unknown effects of inversions can result in cloud heights failing to meet specification.
2. *Characterization of Missing CO_2 Channel*. Our ability to place cirrus properly is in large part determined by our ability to model the observations within CO_2 absorption bands. By including sounder (CrIS) information, we have shown success in better placing cirrus cloud heights. With this information, the ability to perform well in the presence of cirrus clouds is in jeopardy.
3. *Multi-layer clouds*. While the AWG cloud type algorithm does include a multi-layer detection, our knowledge of the properties of that lower cloud is limited.

The Cloud Application Team will continue to be involved in developments that impact the above error sources.

6 PRACTICAL CONSIDERATIONS

6.1 Numerical Computation Considerations

The ACHA employs an optimal estimation approach. Therefore, it requires inversions of matrices that can, under severe scenarios, become ill-conditioned. Currently, these events are detected and treated as failed retrievals.

6.2 Programming and Procedural Considerations

The ACHA makes heavy use of clear-sky RTM calculations. The current system computes the clear-sky RTM at low spatial resolution and with enough angular resolution to capture sub-grid variation to path-length changes. This approach is important for latency consideration as the latency requirements could not be met if the clear-sky RTM were computed for each pixel.

6.3 Quality Assessment and Diagnostics

The optimal estimation framework provides automatic diagnostic metrics and estimates of the retrieval error. It is recommended that the optimal estimation covariance matrices be visualized and analyzed on a regular basis. In addition, the CALIPSO analysis described above should be done regularly.

6.4 Exception Handling

The ACHA includes checking the validity of each channel before applying the appropriate test. The ACHA also expects the main processing FRAMEWORK to flag any pixels with missing geolocation or viewing geometry information.

The ACHA does check for conditions where the ACHA cannot be performed. These conditions include saturated channels or missing RTM values. In these cases, the appropriate flag is set to indicate that no cloud temperature, pressure and height are produced for that pixel. In addition, a fill value is stored for the cloud temperature, pressure and height at these pixels.

6.5 Algorithm Validation

It is recommended that the CALIPSO analysis described earlier be adopted as the main validation tool. If CALIPSO type observations are not available, use of surface-based lidars and radars, such as provided by the Atmospheric Radiation Measurement (ARM) program, is recommended.

7 ASSUMPTIONS AND LIMITATIONS

The following sections describe the current limitations and assumptions in the current version of the ACHA.

7.1 Performance

Assumptions have been made in developing and estimating the performance of the ACHA. The following list contains the current assumptions and proposed mitigation strategies.

1. NWP data of comparable or superior quality to the current 6 hourly GFS forecasts are available. (Use longer range GFS forecasts or switch to another NWP source – ECMWF.)
2. RTM calculations are available for each pixel. (Use reduced vertical or spatial resolution in driving the RTM.)
3. All of the static ancillary data are available at the pixel level. (Reduce the spatial resolution of the surface type, land/sea mask and or coast mask.)

4. The processing system allows for processing of multiple pixels at once for use of spatial texture information. (No mitigation possible)

For a given pixel, should any channel not be available, the ACHA algorithm will not be performed on that particular pixel.

7.2 Assumed Sensor Performance

It is assumed that the ABI sensor will meet its current specifications.   However, the ACHA will be dependent on the following instrumental characteristic:

● Unknown spectral shifts in some channels will cause biases in the clear-sky RTM calculations that may impact the performance of the ACHA.

7.3 Pre-Planned Product Improvements

While development of the baseline ACHA continues, we expect in the coming years to focus on the issues noted below.

7.3.1 Optimization for Atmospheric Motion Vectors

The AMV team is critically dependent on the performance of this algorithm. In addition, the AMV team has a long heritage of making its own internal estimates of cloud-top height. Therefore, it is important that the CAT and AMV teams work together, particularly on the issue of atmospheric inversions.

7.3.2 Implementation of Channel Bias Corrections

The MYD06 development team has found that bias corrections are critical for the proper use of infrared channels for cloud height estimation. Currently, we utilize no bias corrections in ACHA.   In addition, we plan to implement a mechanism to account for the large surface biases in NWP data.

7.3.3 Use of 10.4 μm Channel (for ABI)

The 10.4 μm channel is new to the world of satellite imagers. We expect to incorporate this channel into the ACHA to improve our cloud microphysical retrievals. We expect the GOES-R Risk Reduction projects to demonstrate its use before implementation into the operational algorithm.

8 REFERENCES

Cross J., I. Gladkova, W. P. Menzel, A. Heidinger and M. D. Grossberg, 2013: Statistical estimation of a 13.3-um Visible Infrared Imaging Radiometer Suite channel using multisensory data fusion. J. Appl. Remote Sens. 7 (1), 073473, doi: 10.1117/1.JRS.7.073473

Heidinger, Andrew K. and Pavolonis, Michael J.. Gazing at cirrus clouds for 25 years through a split window, part 1, 2009: Methodology. Journal of Applied Meteorology and Climatology, Volume 48, Issue 6, pp.110-1116

Heidinger, A. K.; Pavolonis, M. J.; Holz, R. E.; Baum, Bryan A. and Berthier, S., 2010: Using CALIPSO to explore the sensitivity to cirrus height in the infrared observations from NPOESS/VIIRS and GOES-R/ABI. Journal of Geophysical Research, Volume 115, 2010, Doi:10.1029/2009JD012152

Heidinger, Andrew K., Y. Li, B. A. Bryan, R. E. Holz, S. Platnick and P. Yang, 2015: Retrieval of Cirrus Cloud Optical Depth under Day and Night Conditions from MODIS Collection 6 Cloud Property Data. *Remote Sensing*, 7(6), 7257-7271

Heidinger, A. K., Bearson, N., Foster, M. J., Li, Y., Wanzong, S., Ackerman, S., Holz, R. E., Platnick, S., and Meyer, K., 2019: Using sounder data to improve cirrus cloud height estimation from satellite imagers, J. Atmos. Ocean. Tech., 36, 1331-1342

Hannon, S. L. L. Strow, and W. W. McMillan, 1996: Atmospheric infrared fast transmittance models: A comparison of two approaches, Proceedings of SPIE, 2830, 94-105.

Hansen, M., R. DeFries, J.R.G. Townshend, and R. Sohlberg, 1998: UMD Global Land Cover Classification, 1 Kilometer, 1.0, Department of Geography, University of Maryland, College Park, Maryland, 1981-1994.

W. P. Menzel, R. A. Frey, B. A. Baum, and H. Zhang, 2006: Cloud Top Properties and Cloud Phase - Algorithm Theoretical Basis Document. Products: 06-L2, 08-D3, 08-E3, 08-M3, NASA Goddard Space Flight Center, Tech. Rep. ATBD Reference Number: ATBD-MOD-05

Seemann, S.W., E. E. Borbas, R. O. Knuteson, G. R. Stephenson, H.-L. Huang, 2008: Development of a Global Infrared Land Surface Emissivity Database for Application to Clear Sky Sounding Retrievals from Multi-spectral Satellite Radiance Measurements. *J. Appl. Meteor. Climatol.*, 47, 1, 108-13

Rodgers, C.D., 1976: Retrieval of atmospheric temperature and composition from remote measurements of thermal radiation. Rev. Geophys. Space Phys., 60, 609-624.

GOES-R Series Ground Segment (GS) Project Functional and Performance Specification (F&PS) [G417-R-FPS-0089]

GOES-R ABI Cloud Mask Algorithm Theoretical Basis Document

GOES-R ABI Cloud Type/Phase Algorithm Theoretical Basis Document

GOES-R Level 1 Requirements Document (L1RD)

GOES-R Series Mission Requirements Document (MRD) [P417-R-MRD-0070]

GOES-R Acronym and Glossary (P417-R-LIST-0142)

Yang, P.; Bi, L.; Baum, B.A.; Liou, K.N.; Kattawar, G.W.; Mishchenko, M.I.; Cole, B, 2013: Spectrally consistent scattering, absorption, and polarization properties of atmospheric ice crystals at wavelengths from 02 to 100 μm. *J. Atmos. Sci. 70*, 330–347.

9 APPENDIX A.   GOES-17 MITIGATION

GOES-17 was moved into operational service as GOES West on February 12, 2019. However, there is a well known issue with the ABI detector cooling system. The loop heat pipe (LHP) system, which cools the ABI detectors, is not adequately maintaining the optimal temperatures. During night times, before and after both equinoxes, the sun heats up several of the ABI infrared detectors and degrades the imagery to the point of being unusable. Two of the channels most affected (12.3 um and 13.3 um) are used as input into the baseline ACHA mode. This in turn degrades the quality of ACHA, and in the worst LHP events, no retrieval is made. Figure 28 shows the GOES-17 ACHA input channels for August 30, 2019 at 1400 UTC during a severe LHP event.
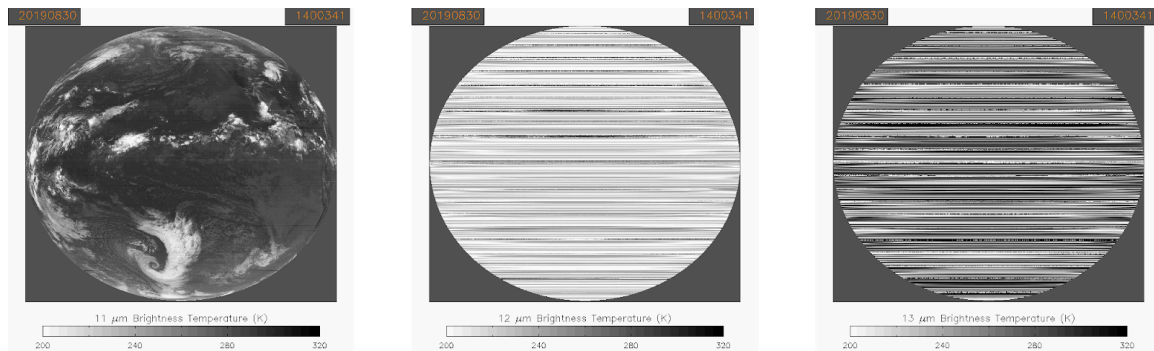

Figure 28 **GOES-17 ACHA input channels on August 30, 2019 at 1400 UTC. The 12.3 and 13.3 um channels will cause the ACHA retrieval to fail.**

The ABI detector cooling system is designed to run at a temperature of 81 K during normal heating days (June 15, 2019). During severe LHP events (August 30, 2019) the temperature may rise to 107 K. This temperature is available in the L1b data as the variable "maximum_focal_plane_temperature". Tim Schmit (NOAA/NESDIS/STAR) designed temperature thresholds for these LHP events. OSPO adopted these on October 2, 2019 at 1704 UTC. Table 7 is from an OSPO bulletin. CLAVRx adopted the Warming Side Threshold, except for Band 14. This was kept at 100.0 K instead of 93.0 K.

Table 7 *ACHA focal plane temperature thresholds for GOES-17 LHP events.*

Band #	Central Wavelength (um)	Warming Side (K) Threshold	Cooling Side (K) Threshold
7	3.89	150.0	150.0
8	6.17	93.0	94.0
9	6.93	93.0	94.0
10	7.34	90.5	91.5

11	8.44	97.0	98.0
12	9.61	89.0	90.0
13	10.33	100.0	101.0
14	11.19	93.0	94.0
15	12.27	92.0	93.0
16	13.27	86.0	87.0

During LHP events the focal plane temperatures from the L1b data, and the focal plane temperature thresholds (see Table 7) are used to determine the "anchor channel" in ACHA. Within the CLAVRx framework, a new module was created to check the thresholds and possibly turn channels off to upstream algorithms (mask, phase, ACHA) if threshold values are exceeded. This module can set the 10.3 um channel as the window channel, leave the 11.2 um channel as the window, and possibly stop processing if both the 10.3 and 11.2 um channels exceed their thresholds. If the 10.3 um channel has been chosen, an internal flag is made available to ACHA.

For GOES-17, ACHA may modify the user requested mode. During LHP events, the mode may change to one using the 3.9 and 11 um channels or 3.9 and 10.3 um channels. The call to ACHA first checks for the 10.3 um use flag and will switch the following 11 um channel variables to 10.3 um values: 1) Channel Index, 2) 11 um brightness temperatures, 3) 11 um radiances, 4) 11 um clear sky radiances, 5) 11 um surface emissivity, 6) 11 um profiles of atmospheric radiances, 7) 11 um profiles of atmospheric transmission, and 8) 11 um black body radiance profiles. It is important to note that this is a night time only mode (~0830 - 1930 UTC).

To assess the change between the baseline ACHA mode (110_120_133) and the new mode (038_110), a night time period of normal focal plane temperatures was chosen (June 2019). This ensured that the cloud mask and phase were identical for both ACHA modes. ACHA was run twice using each of the above modes. Currently, ACHA mode 038_110 suffers from failed water cloud retrievals. This is still being investigated, so temporarily, in the case of failed water cloud retrievals, the software will use the opaque height assignment, in conjunction with the inversion logic to allow some of those failed retrievals back. Figure 29 shows an ACHA cloud top pressure (CTP) image for the two modes. Overall there is decent visual agreement, but ACHA Mode 038_110 shows many more failed retrievals in the upper level clouds (150 - 400 hPa).
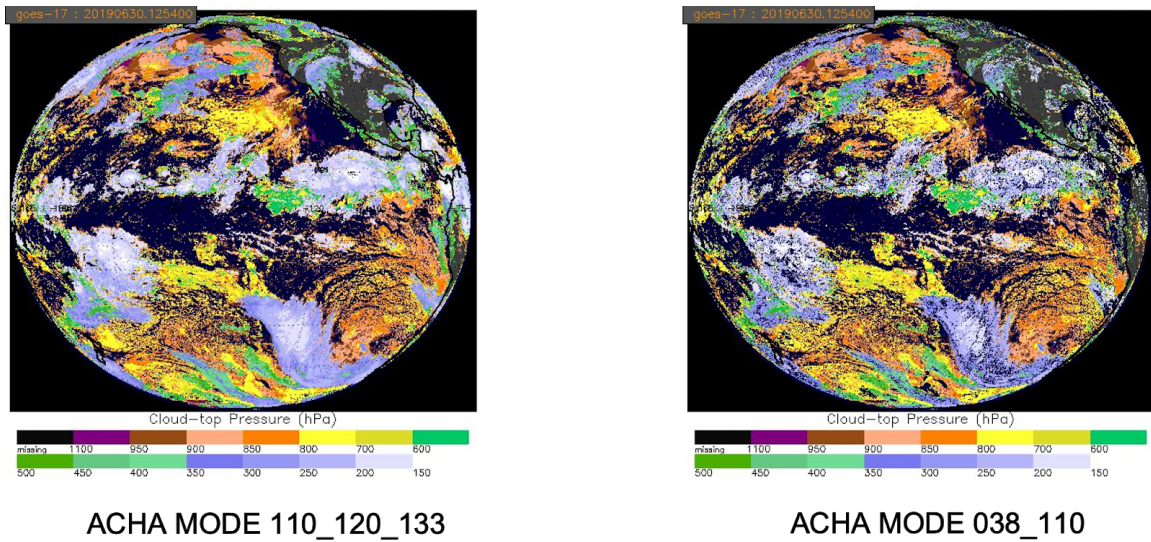
ACHA MODE 110_120_133   ACHA MODE 038_110

Figure 29 **GOES-17 ACHA cloud top pressure for two different modes from June 30, 2019 at 1250 UTC.**

To assess the quality of the new ACHA mode, comparisons to CALIPSO were performed. Seven days of CALIPSO comparisons to ACHA were performed using data from a non-LHP time period. June 1, 6, 11, 16, 21, 26, and 30 were included. 97 collocation datasets were produced. Mode 038_110 will only be attempted at night, so only collocations between 0830 - 1930 UTC were allowed. Collocations were further limited by constraining scan time differences of +/- 12 minutes, GOES-17 sensor zenith angle < 62.

Figure 30 shows the CALIPSO GOES-17 ACHA collocation locations for the June data.
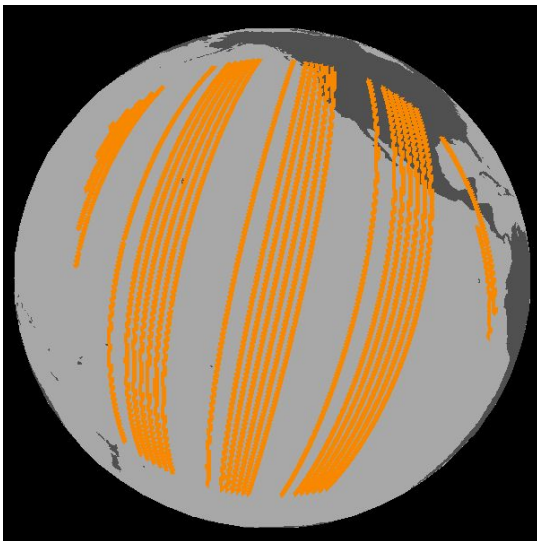

Figure 30 **GOES-17 ACHA CALIPSO collocation locations for June 2019.**

Analysis for the cloud top height (CTH) will be shown in the figures below. Similar results are observed for cloud top temperature (CTT) and cloud top pressure (CTP). GOES-R requirements for CTH include an accuracy (mean difference) of 0.5 km, and a precision (standard deviation) of 1.5 km for all clouds with emissivity of greater than 0.8. One other restriction the cloud team requires is that there only be one cloud layer in the data.
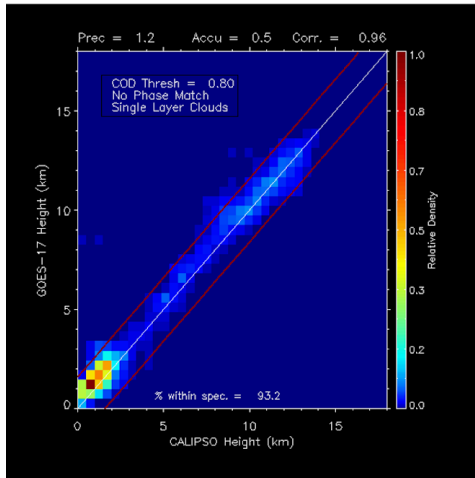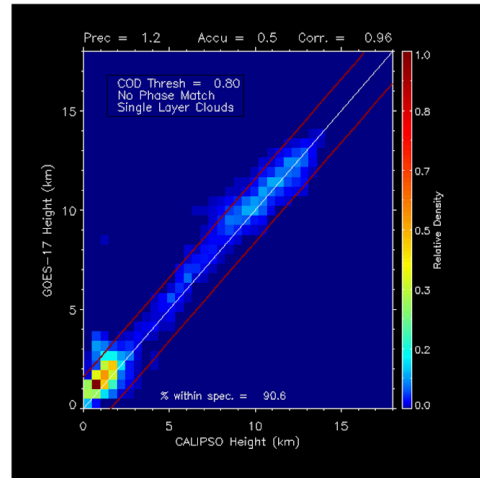
ACHA MODE 038_110   ACHA MODE 110_120_133

Figure 31 **Scatter plots of GOES-17 CTH versus CALIPSO CTH.**

Figure 31shows scatter plots between ACHA CTH and CALIPSO CTH . Both modes, with the above restrictions, are within required specifications. The scatter plots include all phase types. The following figures break out images by cloud phase.

Figure 32 shows histograms of GOES-17 ACHA CTH minus CALIPSO CTH ice clouds only, at differing emissivities. As in Figure 31, the histograms show good agreement between the two ACHA modes.
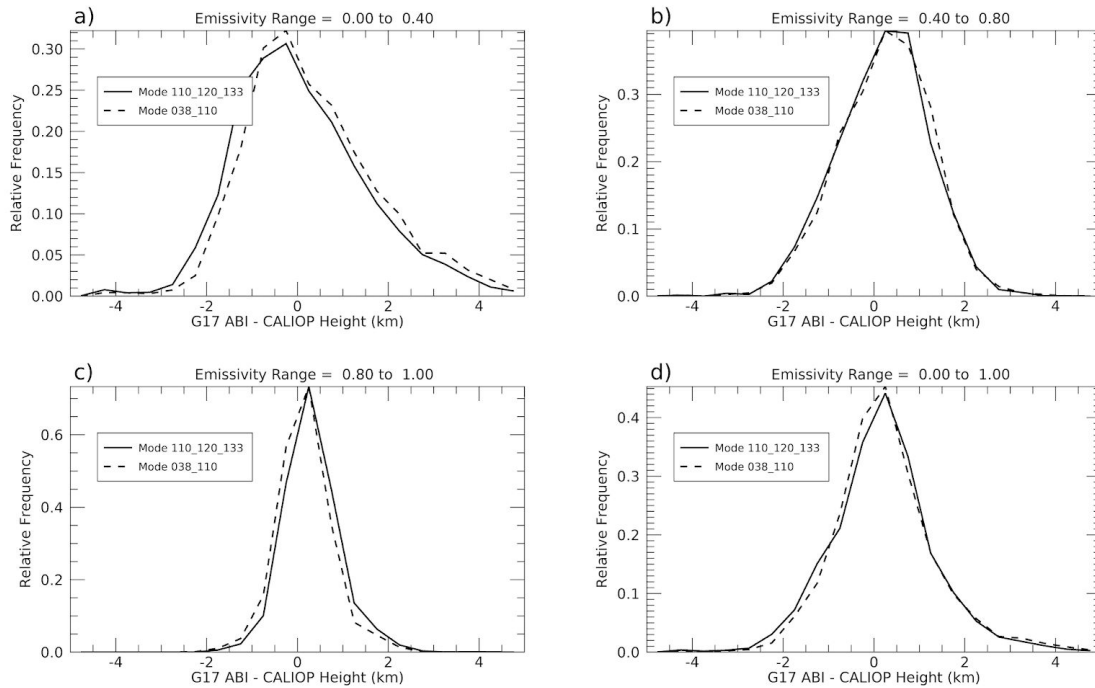
Figure 32 **Histograms of GOES-17 - CALIPSO CTH at various emissivities. Ice clouds only.**

Figure 33 shows histograms of GOES-17 CTH - CALIPSO CTH water clouds only, at differing emissivities. The water cloud plots show even better agreement between the modes than observed in the ice cloud plots of Figure 32.
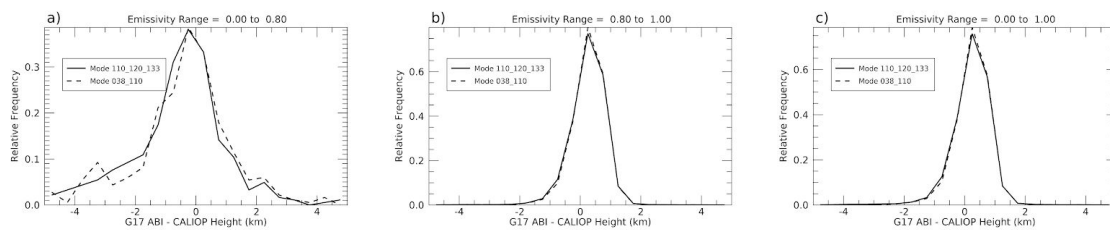

Figure 33 **Histograms of GOES-17 - CALIPSO CTH at various emissivities. Water clouds only.**

The GOES-17 ACHA CALIPSO comparison is an idealized solution. In LHP events, the cloud mask and cloud phase will most likely not be as high quality as it was for the June 2019 dataset, and will lead to degraded quality cloud heights.

The mitigated software has been delivered to NOAA's ASSISTT team for integration into the Framework. The initial software port was completed on November 26, 2019. Testing and sample data comparisons still need to be worked on.